New Particle Formation in a Realistic Daytime Urban Atmosphere:

$SO_2/NO_x/O_3$/Hydrocarbon Air Mixtures

Katherine Elizabeth Galloway

A thesis submitted to the faculty of the University of North Carolina at Chapel Hill in partial fulfillment of the requirements for the degree of Master of Science in the department of Environmental Sciences and Engineering in the School of Public Health

Chapel Hill
2008

Approved by

Prof. Richard M. Kamens, Advisor

Prof. David Leith, Reader

Prof. Jason West, Reader

ABSTRACT

Katherine Galloway

New Particle Formation in a Realistic Daytime Urban Atmosphere:

$SO_2/NO_x/O_3$/Hydrocarbon Air Mixtures

(Under the direction of Richard Kamens, David Leith, and Jason West)

The particle nucleation mechanism of binary mixtures of water and sulfuric acid is of recent interest to the scientific community. To observe sulfuric acid-water induced particle nucleation and growth in a more realistic controlled urban environment, a series of daytime experiments were conducted in the 270 m^3 dual UNC Aerosol Smog Chamber with near-ambient levels of organics in the presence of other atmospheric aerosols and sulfur dioxide. Experimental and modeling results support the theory that stable nucleation and growth in the urban atmosphere are related to gas-phase sulfuric acid. The number of stable nuclei generated in the individual experiments may be approximated by an exponential fit of sulfuric acid and in some cases, toluene. If all the model generated sulfuric acid appears in the particle phase, sulfate would contribute 5 to 25% of the initial burst of the particles, depending on the concentrations of reacting species and the reaction time.

ACKNOWLEDGMENTS

This work is dedicated to my family, friends, and colleagues – your support during the last two years has been tremendous.

I would like to express gratitude to my advisor, Rich Kamens, who generously provided me with a supportive research home. Many thanks to committee members, Dr. David Leith and Dr. Jason West, who gave me welcome guidance along the way.

I could not have conducted this research on my own. Special thanks are due to my lab partners, Rebecca Wilson, Eric Chen, and Yang Zhou, for their creative thinking and countless 4:30 a.m. trips to the smog chamber.

I would like to thank Don Fox, Maryanne Boundy, and Jack Whaley for their encouragement since day one.

I wish to extend my gratitude to the National Science Foundation for their support to this project (A Kinetic Model for Predicting Secondary Organic Aerosol Formation in Complex Hydrocarbon Mixtures).

Matt, my heart, I love you. Why don't we get married, quit our jobs, move across the country, and both go to UNC graduate school?

CONTENTS

LIST OF TABLES

LIST OF FIGURES

LIST OF ABBREVIATIONS

ETH	ethylene
H_2SO_4	sulfuric acid
HNO_3	nitric acid
lpm	liters per minute
nm	nanometer
N and S	North and South
NO	nitric oxide
NO_2	nitrogen dioxide
O_3	ozone
OH	hydroxyl radical
OLE	olefin
PAR	paraffin
ppb	parts per billion
PKSS	Photochemical Kinetics Simulation System
ppm	parts per million
ppmC	parts per million carbon
SA	secondary aerosol
SF6	sulfur hexafluoride
SO_2	sulfur dioxide
SOA	secondary organic aerosol
SMPS	scanning mobility particle sizer
Tg(S)	Teragrams sulfur
Tol	toluene
TSP	total suspended particles
μm	micrometer

CHAPTER I

INTRODUCTION

Atmospheric particles have the potential to affect human health adversely, impair visibility, and alter temperature in the atmosphere through the process of radiative forcing. Particles in the atmosphere scatter and absorb shortwave and long-wave radiation, which in most cases exerts a direct cooling effect of the earth. Aerosols also play an important role in the formation and behavior of clouds by affecting the amount, lifetime, water content, and height of clouds, which can indirectly influence the earth's albedo. Studies indicate that organic aerosol plays an important role in both direct and indirect aerosol forcing; however, aerosols remain the dominant uncertainty in radiative forcing in global climate models (IPCC, 2007, Kanakidou *et al*., 2005, Novakov & Penner, 1993).

Particles in the atmosphere arise from both natural and anthropogenic sources. These particles consist of organic or inorganic constituents, and are either emitted directly (*i.e.*, primary aerosol) or formed in the atmosphere through photochemical processes (*i.e.*, secondary aerosol) (Seinfeld, 1986; Hinds, 1999). The scientific community is predominantly investigating the processes related to the formation and composition of secondary organic aerosol (SOA) (Kanikidou *et al*., 2005). Secondary organic aerosols are formed by the production of non-volatile and semi-volatile gas phase products of organic precursors and photochemical oxidants found in both rural and urban environments. Initially, if the products' gas-phase concentrations exceed their saturation concentration, the vapor

phase products can condense onto existing background particles, forming an organic liquid layer on the particle (Odum *et al.*, 1996). However, once the organics have condensed on the particle, even products whose gas-phase saturation is below their saturation concentrations can partition into the liquid organic layer (Pankow *et al*., 1994; Odum *et al*., 1996). This process is influenced by a given volatile organic compound's atmospheric abundance, chemical reactivity, and volatility of its products (Seinfeld & Pandis, 1998; Pankow, 1994). Secondary aerosol formation (SA) may be defined as chemically generated atmospheric aerosols from inorganic precursors.

Particles can also form in the atmosphere by a process of called nucleation, in which trace substances and water undergo a phase transformation to the liquid or solid phase. Many mechanisms have been proposed for the formation of new particles in the atmosphere. In general, nucleation occurs in the absence or presence of foreign material, often referred to as homogeneous and heterogeneous nucleation respectively (Seinfeld & Pandis, 1998). Some examples of proposed mechanisms include: (a) classical homogeneous nucleation theory based on statistical and thermodynamic arguments (Volmer & Weber, 1926; Seinfeld & Pandis, 1998); (b) oxidation of SOA precursors (often biogenics) in the absence of existing aerosol (Went, 1960); (c) binary mixtures of water and sulfuric acid (Seinfeld & Pandis, 1998; Doyle, 1961; Clark *et al*., 1998; McMurry, 2006); (d) ternary mixtures of water, sulfuric acid, and ammonia (Kulmala *et al.*, 2001); (e) ion induced nucleation of binary, ternary, or organic vapors (Lovejoy *et al.*, 2004; Katz *et al.*, 1994); and (f) oligomer formation via cloud processing (Lim *et al*., 2005; Altieri e*t al.*, 2006).

Of the many nucleation theories proposed, the mechanism of binary mixtures of water and sulfuric acid is of recent interest to the scientific community. In 1992, Weber and McMurry analyzed nucleation events at a remote site at the Mauna Loa Observatory, Hawaii. They observed bursts in ultrafine particles accompanied by peaks in gas-phase sulfuric acid measurements (Weber & McMurry, 1992). Analysis of measurements taken from a boreal forest in Finland suggests that the most likely source of nucleated particles in that area was formed by a water-sulfuric acid-ammonia mechanism (Kulmala *et al.*, 2001; Jansen *et al.*, 2001). More recently, analysis of particulate submicron sulfate measurements taken during the Mediterranean Intensive Oxidant Study was attributed to gas-phase sulfuric acid formation (Mihalopoulos, 2007) Analysis of national ambient fine particulate matter data indicate that sulfate can comprise up to 25% of fine particulate matter mass in regions of the United States (Blanchard *et al.*, 2007).

Seinfeld and Pandis state that the most important binary nucleation system in the atmosphere is that of sulfuric acid and water, and uphold Doyle's theory that extremely small amounts of H_2SO_4 nucleate subsaturated water vapor (Seinfeld & Pandis, 1998). After initial nucleation, it has been theorized that the major part of the growth is due to condensation of organic vapors (Gao *et al.*, 2001, Gaydos *et al.*, 2004). The particles that are generated in this system would contain an inorganic sulfur-based core with an organic liquid layer, and would thus represent a more complex classification of SA/SOA. A recent review of H_2SO_4 nucleation suggest the rate at which observable atmospheric stable nuclei are generated may be approximated by a direct function of the H_2SO_4 gas phase concentration to some power between one and two (McMurry, 2006). A pre-exponential factor on the $[H_2SO_4]$ term is used to describe the additional impact of organics.

Many of the nucleation theories presented have been observed either in laboratory experiments or derived from first principles. Of the SOA laboratory experiments conducted to date, experiments performed in small scale reaction vessels and larger scale smog chambers have been conducted with initial concentrations of some oxidants *(i.e.*, OH, NO_x, SO_x, etc.), single or binary mixtures of hydrocarbons *(i.e.*, toluene, α-pinene, d-limonene, isoprene, etc.) in either day-time or night-time conditions. However, concentrations typically used in laboratory experiments are higher than those observed in the environment, and experiments rarely use pre-existing aerosol (Kulmala, 2003). If concentrations of nucleating vapors are high in laboratory experiments, the vapors can be responsible for growth by condensation. The complexity of this process makes it difficult to quantify the transition between initial nucleation and growth.

It is estimated that global sulfur emissions range from 98-120 Tg(S) yr^{-1}. Of that, approximately two-thirds originates from anthropogenic sources (primarily fossil-fuel combustion), and one-third is naturally occurring (Seinfeld & Pandis, 1998). In an urban environment, gas-phase sulfuric acid often originates from reactions of anthropogenic emissions of sulfur dioxide with hydroxyl radicals (OH) generated from hydrocarbons and/or oxides of nitrogen.

To observe sulfuric acid-water induced particle nucleation and growth in a more realistic and complex controlled urban environment, a series of six daytime experiments were conducted in a large outdoor smog chamber using near-ambient levels organics in the presence of other atmospheric aerosols and sulfur dioxide. To provide a realistic source of urban hydroxyl radicals to oxidize sulfur dioxide to gas-phase sulfuric acid, a unique eleven-component gas-phase mixture of hydrocarbons was created. This mixture, which we term the "UNC mix", approximates ambient mixtures commonly found in urban air environments. To our knowledge, the reaction of sulfur dioxide in dilute urban smog mixtures has not been studied.

CHAPTER II

EXPERIMENTAL METHODS

Experiments were conducted in the University of North Carolina (UNC) 270 m^3 dual outdoor aerosol smog chambers in Pittsboro, North Carolina. In the dual chamber, matched experiments were conducted with equal initial concentrations of nitric oxide (NO), nitrogen dioxide (NO_2), ozone ($O_{3)}$, hydrocarbons, and background aerosol with usually only one side of the chamber containing an initial concentration of SO_2. The chamber has a Quonset hut design with a surface to volume ratio of 1.08. By convention, one side of the dual chamber is designated North and has a volume of 138 m^3, the other is named South and has a volume of 136 m^3. The laboratory containing all sampling equipment is located beneath the chamber with sampling lines less than 1 m long. A detailed description of the chamber may be found elsewhere (Lee *et al.*, 2004). The experiments were conducted under daylight conditions with temperatures ranging from 270 to 305K, variable humidity from 25-100%, and clear skies.

At the start of each experiment (before sun-up), all gas phase injections were made to the chamber. Sulfur hexafluoride (SF6) was injected into each side of the chamber and monitored by chromatography for its use as a dilution tracer. First, oxides of nitrogen (NO_x) were injected from high pressure cylinders in nitrogen. Ozone and oxides of nitrogen were measured by uv and chemiluminescent monitors (model 49 P/S, Thermo-Environmental Instruments, Indianapolis, IN and ML9841A Tyledyne, Los Angeles, CA) and data was

logged every minute. Ozone, NO, and NO_2 were calibrated by gas phase titration using a National Institute of Standards and Technology (NIST) traceable NO tank before each experiment. Measured amounts of pure liquid phase toluene were heated into a u-tube and volatilized into the chamber and flushed by a nitrogen stream for approximately two minutes. On occasion, the chamber injection manifold was also heated to prevent condensation during cooler temperatures. Descriptions of instruments used for the measurements of oxides of nitrogen, ozone, solar irradiance, temperature and humidity are provided elsewhere (Leungsakul *et al.*, 2004 a and b).

Figure 1. UNC Aerosol Smog Chamber

Next, a gas-phase mixture of volatile hydrocarbons (ranging in volatility from ethylene to trimethylpentane) was injected simultaneously into both sides of the chamber from a high pressure cylinder. This mixture will be called the "UNC mix" and its composition is given in Table 1. Historically, this mixture has been used at the UNC Smog Chamber facility since 1973. It was based on an EPA analysis of the Las Angeles and Cincinnati atmosphere in the late 1960s. This mix was a compromise between actual urban early morning analysis and what could be easily analyzed with a gas chromatograph at that time (Jeffries *et al*, 1975).

The UNC mix consists of 71% paraffins and 29% olefins; aromatic compounds are not included in the mix, but were present in the experiments by liquid injection of toluene.

Table 1. UNC Mix Composition

Compound Name	Percent Carbon Composition	CB4 Composition
isopentane	14.8	5*PAR
n-pentane	25.3	5*PAR
2-methyl-pentane	10.0	6*PAR
2,4-dimethyl-pentane	8.6	7*PAR
2,2,4-trimethyl-pentane	12.0	8*PAR
1-butene	2.5	OLE + 2*PAR
cis-2-butene	3.1	2*CCHO
2-methyl-butene	3.5	OLE + 3*PAR
2-methyl-2-butene	3.2	CCHO + 3*PAR
ethylene	11.7	ETH
propylene	5.2	PAR + OLE

After confirming injected concentrations of hydrocarbons, gas-phase SO_2 was injected by high pressure cylinder in nitrogen. SO_2 was measured by a pulsed fluorescence SO_2 analyzer (Thermo Electron model 43S, Hopkinton, Mass.) and logged every minute. The SO_2 analyzer was calibrated by injecting into the chamber known amounts of a 1010 ppm SO_2 in nitrogen mixture from a NIST traceable SO_2 gas tank.

At the beginning of each experiment, background particle size distribution data were collected by two Scanning Mobility Particle Sizers (SMPS) composed of Differential Mobility Analyzers and Condensation Particle Counters (TSI 3080 with CPC TSI 3022A and TSI 3071 with CPC TSI 3025A, Shoreview, MN). As discussed later in the Results section, bursts of post-nucleation particles were observed by SMPS after SO_2 injection and were not observed when SO_2 was absent. By convention, the SMPS capable of running in a high-flow mode (*i.e.*, 15 lpm) and detecting particles in the 6 to 220 nm range was used to observe

initial nucleation in the chamber that contained SO_2. The TSI 3071 instrument that operated only in a low-flow mode (*i.e.*, 3 lpm) and could measure particles in the 14-690 nm size range was used in the chamber that did not contain SO_2.

As a laboratory practice, SMPS and CPC calibrations are routinely conducted using monodisperse polystyrene latex spheres sized as small as 90 nm, and can be found in Appendix C. Other primary methods of instrument calibration that have been referenced include the electrostatic classification method, which involves generating a polydisperse aerosol with an atomizer and extracting particles within a narrow size range using a differential electrical mobility classifier, calibration of the CPC by direct measurement of a monodisperse aerosol, collecting particle samples on a substrate and then counting them under an electron microscope, and collecting samples on a substrate and measuring mass (Agawal *et al.*, 1978). Historically, the lab group has conducted studies comparing high SMPS particle mass concentrations with gravimetric masses, and has found a good comparison. The other calibration methods listed have been too costly to conduct.

For some experiments, particle sulfate samples were collected simultaneously by a denuder-filter sampling train that consists of two annual denuders in series coated with a solution of 1% Na_2CO_2, 1% glycerin in a 50:50 mixture of H_2O:methanol in the first and 1% citric acid, 1% glycerin in methanol in the second, followed by particle collection on a 47 mm Teflon filter. This system removed gas-phase sulfate from the air stream and facilitated analysis of particle-phase (only) sulfate via ion chromatography (Possanzini *et al.*, 1983; EPA, 1988). Particle sulfate samples were used to verify model predictions of sulfuric acid. The final measured sulfate of the filters was consistent with final model predicted sulfate for high concentrations of initial SO_2 (*i.e.* 0.086 ppm SO_2), but the filter samples suggested a

more rapid increase in sulfate than did the model. For low initial SO_2 concentrations (*i.e.* less than 0.02 ppm SO_2) the method was not sensitive enough to measure sulfate concentrations. Additional information can be found in Appendix D.

CHAPTER III

MODEL DESCRIPTION

Ambient gas-phase sulfuric acid is difficult to sample and measure because of its reactive nature. Typically, sulfuric acid is sampled in conjunction with aerosols in a complex sampling train consisting of a coarse particle separator, a quartz or Teflon filter, and a denuder system (EPA, Method 8). Difficulties encountered in collecting samples for acid measurements include sorption losses onto filters, and equilibrium-driven loss or gain of species as a result of nonsteady-state conditions in the atmosphere of the time period of measurement (Lioy & Waldman 1989, ATSDR 1998). After sample collection, acid aerosols are extracted from the filter and analyzed for ions. Sulfuric acid in air can also be measured by a continuous flame photometric detector; however this method is unable to discriminate between sulfur species (Appel *et al.*, 1987, ATSDR 1998). EPA Method 8 is the only method EPA has published for measuring sulfuric acid; however, it cannot be used because sulfur dioxide and ammonia present in the chamber are interfering agents for the method (EPA, Method 8).

Because of the difficulties associated with sampling gas phase sulfuric acid in the smog chamber, a photochemical model using the Carbon Bond 4 (CB-4) photochemical mechanism (Gery *et al.*, 1989) in a simple box model kinetics solver, Photochemical Kinetics Simulation System (PKSS, Jeffries, 1990) was used to predict gas-phase sulfuric acid. PKSS is a collection of programs for computing the concentrations of photochemically generated

species as a function of time (PKSS, Jeffries, 1990). In addition to the existing photochemistry in the CB-4 mechanism, a new condensed toluene mechanism that represents gas-phase products from the photo-oxidation of toluene and further reactions of these products with atmospheric oxidants (Hu *et al*., 2007) and relevant SO_2 reactions were added. The complete mechanism may be found in Appendix A.

Toluene Chemistry

The condensed toluene mechanism (Kamens mechanism under development, May 2008) was based on the aromatic summary mechanistic work of Calvert *et al*., (2002) which explicitly represents the formation of first-generation gas-phase products 2-butenedial, 4-oxo-pentenal, glyoxal, and methylglyoxal from the photo-oxidation of toluene and further reactions of these products with atmospheric oxidants. Based on the work of Hu *et al*., (2007), Kliendiest *et al*., (2004), and Edney *et al*., (2001), four major product groups lead to secondary organic aerosol. There are: (a) polymers of glyoxal and methylglyoxal (glypoly), (b) hydroxynitrophenols (OHNO3Phenols), (c) aliphatic hydroxy nitrates and acids ($OHcarbNO_3$), and (d) highly oxygenated C4 and C5 aliphatics (polycarb). Glyoxal and methylglyoxal from the gas phase were shunted directly to the particle phase as per Hu *et al*., (2007). OHNO3Phenols, $OHcarbNO_3$, and polycarb, were permitted to partition on the particle phase as per Kamens *et al*., (1999, 2001). Background aerosols in the chamber were represented as a general class called seed. A list of the specific toluene reactions used in this study is given in Appendix A.

Chamber Wall Chemistry

For experiments conducted in smog chambers, it is well established that heterogeneous processes occurring on the walls can influence the behavior of the chemical system (Killus & Whitten, 1990; Carter *et al*., 1981, Hu *et al*., 2007). As described elsewhere, a series of wall-characterization experiments have been conducted to quantify the reactivity of the walls at the UNC Aerosol Smog Chamber (Kamens *et al*., 1999). In addition to wall loss rates of previous compounds studied in the smog chamber, additional day and night-time characterization experiments were performed to determine wall loss rates for sulfur dioxide. A typical loss of SO_2 to the walls was 100x faster than that of ozone, with SO_2 exhibiting a half life of 1.5 to 3 hours, even at night. Figure 2 illustrates the decay of SO_2 at night. SO_2 was assumed to react with a certain number of wall sites. As the wall sites became satisfied with SO_2, they are reacted away; the number of these sites is assumed to be a function of chamber of relative humidity. Hence, this is represented as a second-order rate process with a rate constant of 0.01 ppm^{-1} min^{-1}. As observed by the SO_2 wall loss characterization experiments, approximately 95% of the SO_2 was reacted to the walls in the model. Even though the walls are a major loss of SO_2 in the system, there was ample SO_2 present in the chamber to induce nucleation during the experiments (on average 0.02 ± 0.01 ppb), as discussed later in the results section. Further, for an average OH concentration of 1×10^6 radicals cm^{-3}, the natural lifetime of SO_2 with respect to the OH reaction only is approximately 13 days, or a 1% SO_2 decay per hour (Pitts & Pitts, 2000).

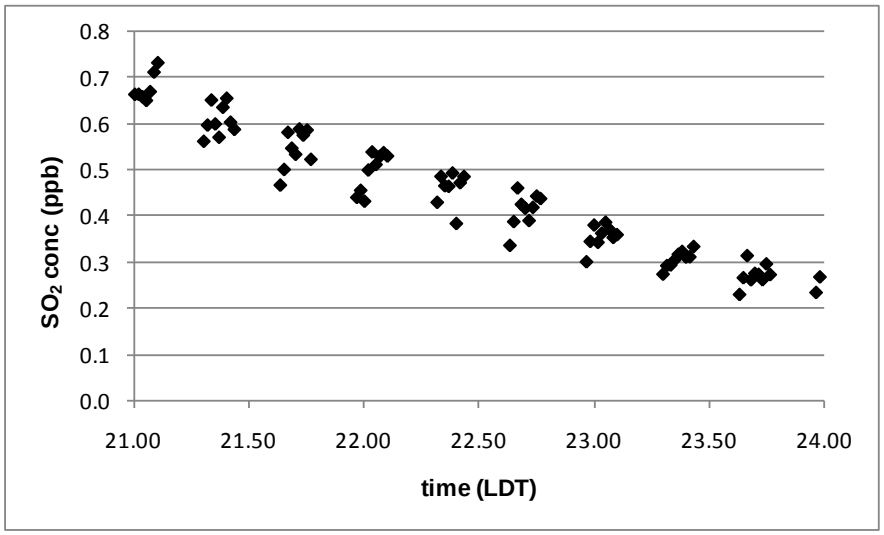

Figure 2. SO_2 nighttime decay.

For the six experiments, the SO_2 rate constant adequately fit the measured SO_2 data except when there was a high concentration of water in the chamber (high relative humidity), indicated by the presence of condensation on the inner chamber walls. In those situations, the rate at which SO_2 was lost to the walls was manually adjusted by a factor of 2, and confirmed by comparison with SO_2 measurements. An auxiliary mechanism containing all of our unique smog chamber effects is included in the PKSS model (Jeffries *et al*., 1999; Voicu, 2003).

Sulfuric acid is soluble in water, and therefore would be lost to the walls at a higher rate than sulfur dioxide. Assuming that sulfuric acid behaves similarly to nitric acid on the Teflon chamber walls, the wall loss mechanism for nitric acid used for the EUPHORE smog chamber as modeled in the Morpho mechanism was used as a reference (Jeffries *et al.*, 2003) In the Morpho model for the EUPHORE chamber, the first order dry rate constant for nitric acid is 8.2×10^{-5} /sec, yielding a first order HNO_3 rate coefficient to the walls under dry conditions of approximately 5×10^{-3}/min in the EUPHORE chamber. Since the UNC Aerosol

Smog Chamber has a higher surface to volume ratio than the EUPHORE chamber, it was assumed that the UNC chamber has twice the loss, or $10x10^{-3}$/min. The ratio of the surface area of the UNC Dual Aerosol Smog Chamber to the EUPHORE chamber is approximately 292 m^2: 199 m^2 or 1.5. Converting the first-order H_2SO_4 wall loss rate constant to a second-order rate constant by dividing by 1ppm of wall sides yields a second order rate constant of 0.01 ppm^{-1} min^{-1}

Since the six experiments in the study were conducted under humid conditions (25-100% RH), it was assumed that sulfuric acid would be lost to the walls at a faster rate than under the dry conditions used in the EUPHORE comparison. By conducting a sensitivity analysis of varying the sulfuric acid wall loss by a factor of 1-10 times that of the HNO_3 wall loss, a second-order H_2SO_4 wall loss rate constant of 0.04 ppm^{-1} min^{-1} was chosen instead of 0.01 ppm^{-1} min^{-1}. Results of the sensitivity analysis indicate that in the 95% confidence interval of mean values, the predicted H_2SO_4 concentrations can vary by up to 47%.

Sulfur Dioxide Chemistry

The SO_2 reactions and rate constants used in the analysis are given in Table 2. As stated in Pitts & Pitts, (2000), the actual mechanism for the reaction of SO_3 to H_2SO_4 is unknown; however, it appears that SO_3 forms a complex with H_2O, and that H_2O-SO_3 complex reacts with a second water molecule, leading to H_2SO_4. For this reason, the reaction is represented as $SO_3 + 2H_2O \rightarrow H_2SO_4$ in the model. Most recent literature does not provide a rate constant for the reaction of SO_3 to H_2SO_4; however, it is given that the reaction occurs very quickly (Pitts & Pitts, 2000). For this model, a rate constant of 10^{-8} $ppm^{-1}min^{-1}$ was assigned for the reaction $SO_3 + 2H_2O \rightarrow H_2SO_4$.

Table 2. SO_2 reactions

Reaction	Rate Constant ($ppm^{-1}min^{-1}$)
$SO_2 + OH \rightarrow SO_3 + HO_2$	1370 (Stockwell, 1990)
$HO_2 + SO_2 \rightarrow OH + SO_3$	1.3 (Mallard *et al*., 1993)
$SO_3 + 2H_2O \rightarrow H_2SO_4$	(fast) 10^{-8} (est. Pitts & Pitts, 2000)
$SO_2 \rightarrow$ walls	0.01
$H_2SO_4 \rightarrow$ walls	0.04

CHAPTER IV

RESULTS AND DISCUSSION

Experimental Results

In the dual chamber, matched experiments were conducted with equal initial concentrations of NO, NO_2, O_3, hydrocarbons, and background aerosol with only one side of the chamber containing an initial concentration of SO_2. Before sunrise, NO, UNC Mix, SO_2, and toluene were injected into the chamber to supply the OH radicals necessary for photochemical reactions to occur. Figures 3 and 4 show the typical temporal evolution of ozone (O_3), nitric oxide (NO), nitrogen dioxide (NO_2), sulfur dioxide (SO_2), and toluene for a representative experiment. Table 3 lists the initial conditions for each experiment, and Table 4 provides a reference for trace species concentration in the clean troposphere and polluted urban air (Seinfeld, 1986). The experimental conditions span a range of temperatures from 270 to 305K, and relative humidity from 25-100% during clear daylight conditions.

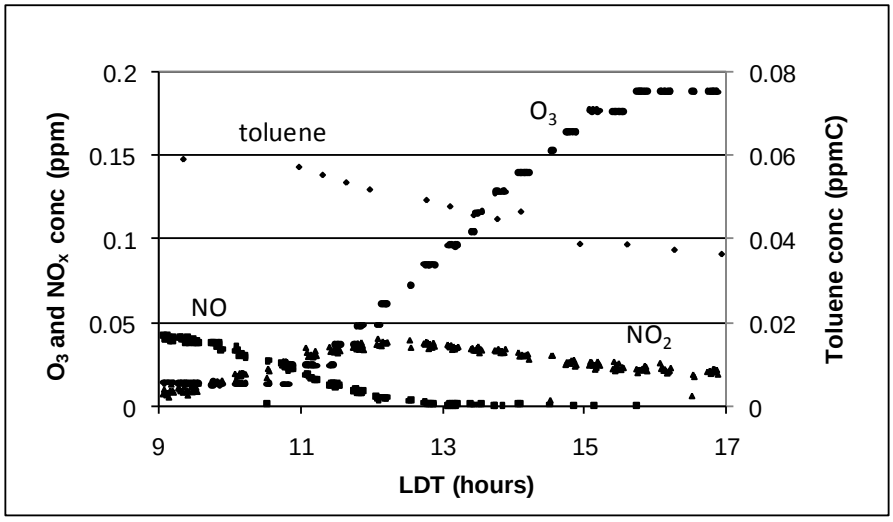

Figure 3. Measured concentrations of NO_x, O_3, and toluene for 021508N experiment. The circles are measured O_3; triangles are measured NO_2; squares are measured NO; diamonds are measured toluene.

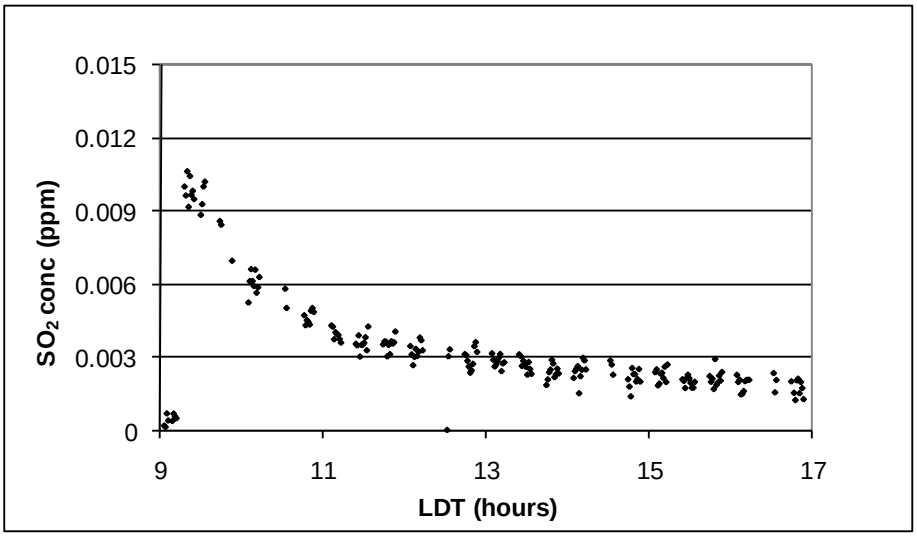

Figure 4. Measured concentrations of SO_2 for 021508N experiment.

Table 3. Experimental Conditions

Experimental Date	Initial Concentration (ppm)					
	$[SO_2]$	[NO]	$[NO_2]$	[Tol](ppmC)	[UNC Mix](ppmC)	[particle mass]($\mu g/m^3$)
101307N*	0.015	0.099	0.003	0.67	2.0	3.2
102107N	0.019	0.059	0.003	0	1.5	2.5
102107S	0	0.057	0.003	0.67	1.5	2.5
020808N	0.029	0.106	0.005	0.67	2.0	3.0
020808S	0	0.106	0.005	0.67	2.0	3.5
021508N	0.011	0.040	0.010	0.40	1.0	2.5
021508S	0	0.040	0.010	0.40	1.0	3.8
030608N	0.086	0.100	0.006	0.67	2.0	2.0
030608S	0.038	0.096	0.003	0	2.0	2.0
031308N	0	0.060	0.040	0.67	2.0	2.5
031308S	0.008	0.060	0.040	0.67	2.0	2.5

*N = North; S = South

Table 4. Trace Species Concentration in the Clean Troposphere and Polluted Urban Air

Species	Marine Boundry Layer (ppb)	Urban Air (ppb)
SO_2[a]	0.02-0.05	up to 200+
NO_x[a]	0.02-0.04	10-1,000
O_3[b]	20-80	100-500
NMHC[b] (non-methane hydrocarbons)		500-1200
Particulate Matter[b] (concentration)	< 20 $\mu g/m^3$	up to 2000 $\mu g/m^3$
Particulate Matter[b] (number concentration)	100 cm^{-3}	100,000 cm^{-3}

a: Seinfeld & Pandis, 1998, b:Seinfeld, 1986

Nucleation

Figures 5 and 7 provide time evolution graphs of observed particle number distribution and show the initial appearance of post-nucleation particles (6-10 nm) followed by coagulation. The particle size distribution was measured over a period of three minutes. Due to the time lag between scans, the data points plotted represent the maximum number of particles measured during the scan. In all experiments, bursts of post-nucleation particles were observed by SMPS approximately one hour after SO_2 injection and were not observed when SO_2 was absent.

The generation of particles and the growth in the particle size distribution in the presence and absence of SO_2 is illustrated in Figures 5 and 7. In the 021508S experiment shown in figures 5 and 6 (SO_2 absent), no burst of new particles was observed, and the number of particles measured by the TSI in low flow mode (14 nm < particles < 660 nm) increased from 650 particles/cm^3 initially to 4,000 particles/cm^3. Additional sampling was conducted in high-flow mode to verify the absence of particles smaller than 14 nm. In the 021508N experiment shown in Figures 7 and 8, the number of fine particles as measured by the TSI with CPC in high flow mode (6 nm < particles < 220 nm) increased from a background level of 650 particles/cm^3 to over 10,000 particles/cm^3 within one hour, and 24,000 particles/cm^3 in 1.5 hours. Additionally, Figures 9 and 10 represent experiments in which different concentrations of SO_2 were injected into both sides of the chamber; in both cases, the number of post nucleation particles observed was higher in the chamber with the higher concentration of SO_2. These observations support the theory that stable nucleation in the atmosphere may be related to gas-phase sulfuric acid.

After observing the appearance of larger particles that contribute to particle mass, the TSI was switched to a low-flow mode in all experiments to measure particle sizes ranging from 14 to 660 nm. Post-nucleation particles continued to grow until coagulation and wall losses dominated the system, at which time the geometric mean diameter of the polydisperse aerosol increased and total number of particles decreased during the remainder of the experiment.

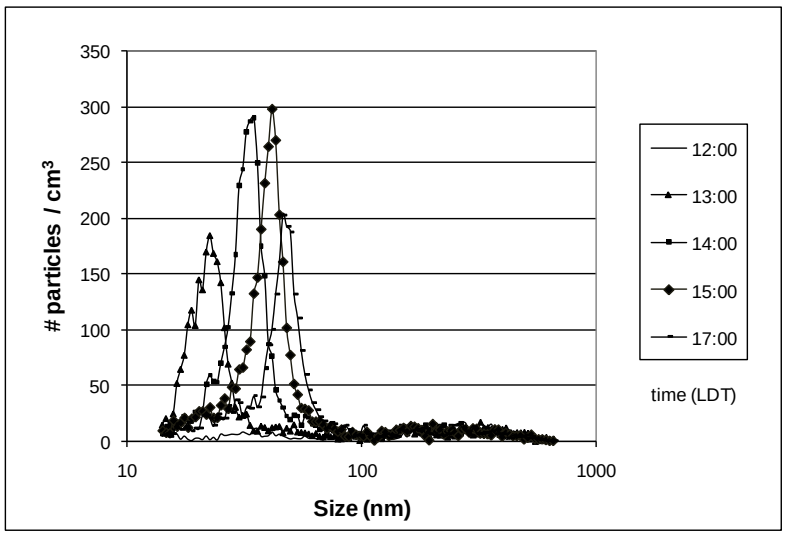

Figure 5. Instantaneous number of particles/cm^3 as measured by low-flow SMPS (14 nm<particles<600 nm) during 021508S experiment (SO_2 absent).

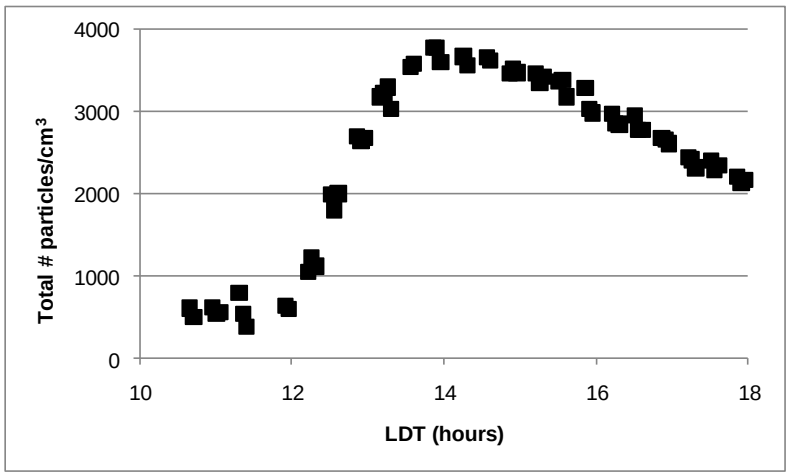

Figure 6. Measured particle number concentration for 021508S experiment (SO_2 absent). Measurements made by SMPS in low-flow mode.

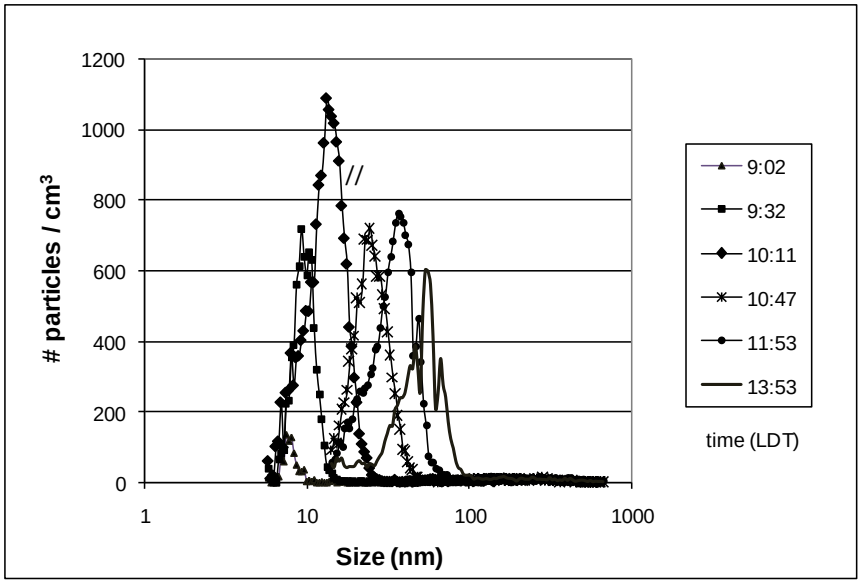

Figure 7. Instantaneous number of particles/cm^3 as measured by SMPS during 021508N experiment (SO_2 present). Measurements taken until 10:00 in high-flow mode (6 nm< particles<220 nm); after 10:00, in low-flow mode.

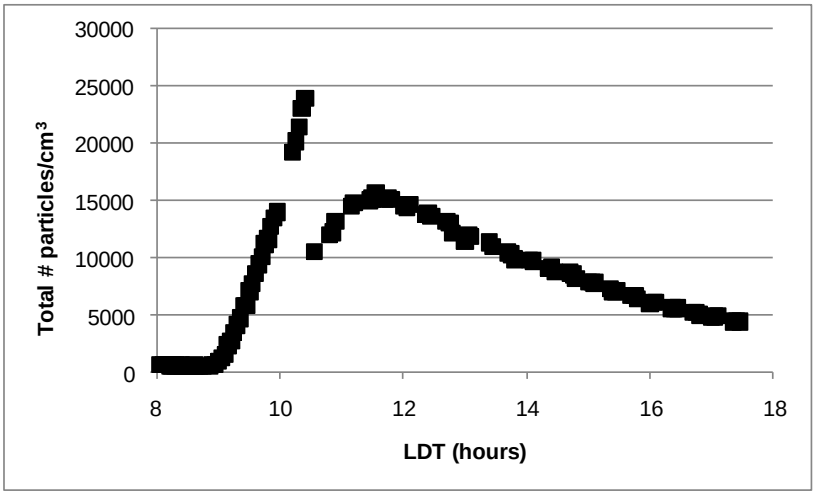

Figure 8. Measured particle number concentration for 021508N experiment (SO_2 present). Measurements collected until 10:00 were collected in SMPS high flow mode; after 10:00 in low-flow mode.

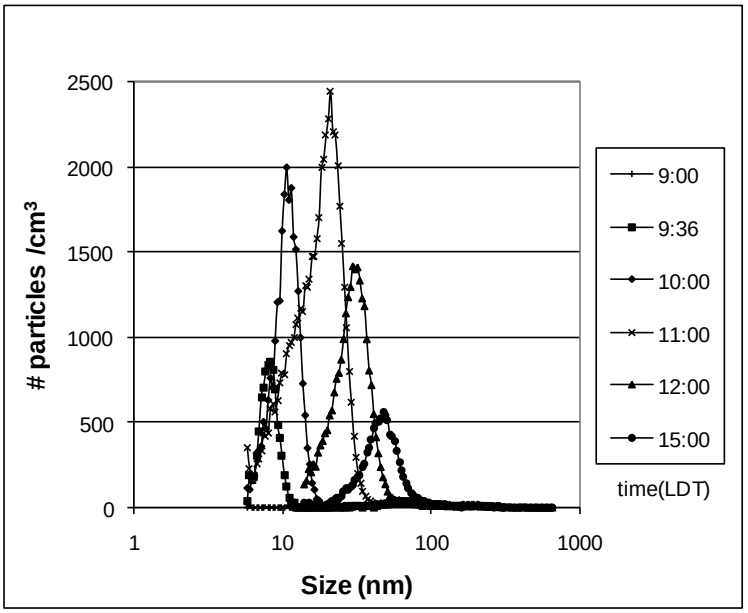

Figure 9. Instantaneous number of particles/cm^3 as measured by SMPS high-flow mode during 030608S experiment. Initial SO_2 injection was 0.038 ppm. Measurements taken until 11:00 in high-flow mode (6 nm< particles<220 nm); after 11:00, in low-flow mode.

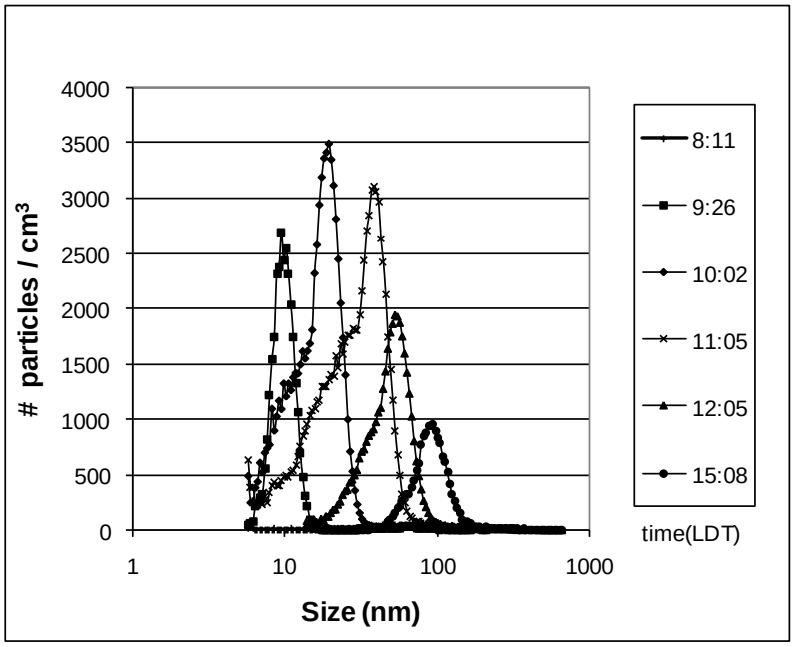

Figure 10. Instantaneous of particles/cm^3 as measured by SMPS high-flow mode during 030608N experiment. Initial SO_2 injection was 0.086 ppm. Measurements taken until 11:05 in high-flow mode (6 nm< particles<220 nm); after 11:05, in low-flow mode.

After the experiments were conducted, it was observed that there was some discrepancy between the number of particles measured by the SMPS and CPC when it was toggled from high-flow to low-flow modes. As illustrated in Figure 8, when the SMPS was in high-flow mode until approximately 10:23, approximately 24,000 particles/cm^3 were observed. The peak in the particle concentration at that time was at 1200 particles of size 16 nm. Since the peak in the particle concentration was within the range of the low-flow mode (14 nm < particles < 660nm) and the total mass of the particles is primarily influenced by the larger particles, the SMPS and CPC were switched to the low-flow mode. Figure 11 shows that as the SMPS was switched to low flow mode 9 minutes later, the peak observed in the particle concentration data was 660 particles of a size 19.5 nm and the total number concentration of particles was 10,500 particles/cm^3. Although it would be expected that the geometric mean diameter of the polydisperse aerosol would increase during nucleation and that the total number of particles observed could decrease due to coagulation, the discrepancy observed in the SMPS data is so large, it is likely due to instrumentation errors. The observed total particle concentration varies by a factor of 2 between the different modes; whereas, specifications for the instrument are given to be ± 10% for the given particle concentration.

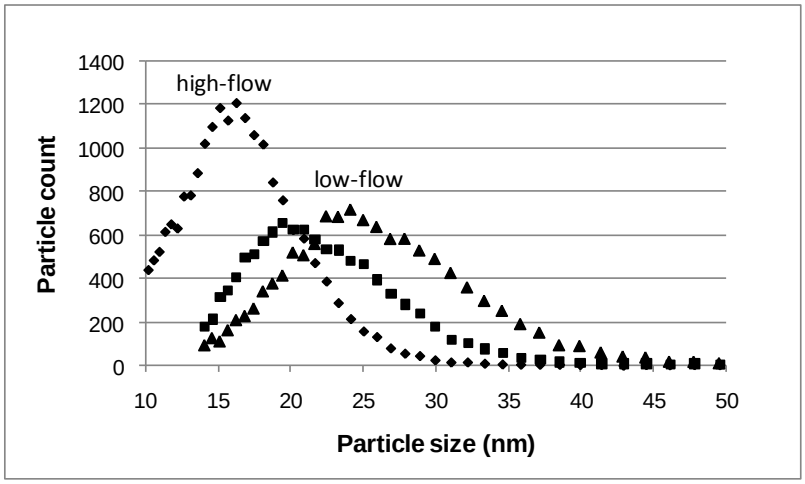

Figure 11. Comparison in particle count in high vs. low flow modes. Diamonds are particles observed in high-flow at 10:23; squares are particles observed in low-flow at 10:32; triangles are particles observed in low flow at 10:47.

The discrepancy between the high and low flow size distributions is currently being investigated by the Kamens research group. Particle sizing calibrations have been conducted with PSL spheres as small as 90 nm, but the discrepancy appears in counting particles smaller than 90 nm. For the analysis presented in this work, please note that any data that was collected in high-flow mode is only compared to data from other experiments conducted in high-flow mode, and the same is true for data collected in low-flow mode.

Nucleation rate

The particle nucleation rates were obtained by taking the time derivative of the fine particle concentration during particle growth as described by a linear fit of particle concentration. Figure 12 illustrates the nucleation rate for 021508N, indicating that the nucleation rate was 4.4 particles cm^{-3} sec^{-1}. Nucleation rates as measured by high-flow SMPS for selected experiments are given in Table 5.

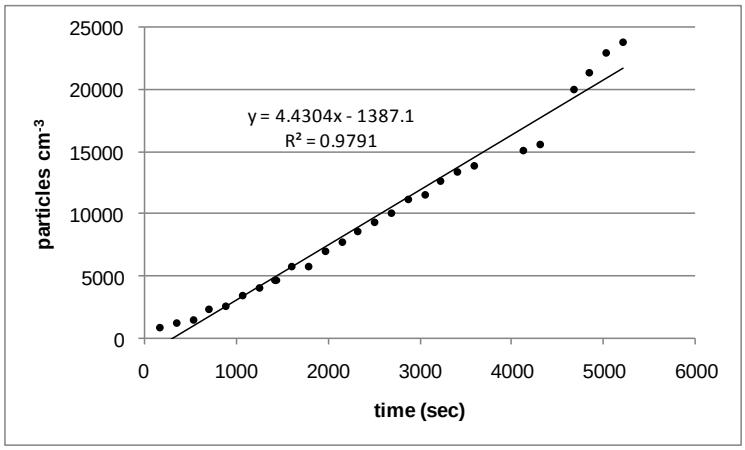

Figure 12. Nucleation rate for 021508N. Circles represent measurements made by SMPS in high flow mode; solid line is linear regression.

Table 5. Various Experimental Nucleation Rates

Date	particles cm^{-3} s^{-1}
021508N	4.4
030608N	15.4
030608S	9.7
031308S	16.8

Model Results

In general, the simulation predicted NO and NO_2 very well (+/- 5%) and under-predicted ozone in all scenarios by 10-20%. Figure 13 illustrates the model fit for O_3, NO, NO_2, and toluene for the 021508N experiment. The simulated decay of toluene was compared with gas chromatography measurements. The condensed mechanism predicted the initial decay of toluene very well; however, the model overestimates the loss of toluene later in the day by up to 30%. In previous studies, the explicit kinetic mechanism to predict SOA formation from

photo-oxidation of toluene developed by Hu *et al*. generally predicted the decay of toluene very well, except in some circumstances in which it overestimates the loss of toluene by 17% (Hu *et al*., 2007). This is a vast improvement over the original CB-4 chemistry which greatly underestimates toluene decay after initial reaction with OH. As in the Hu et al. mechanism, we are using the novel acylperoxy reaction with toluene (Broyles & Carpenter, 2005) to improve the toluene decay beyond that predicted by just OH reactions.

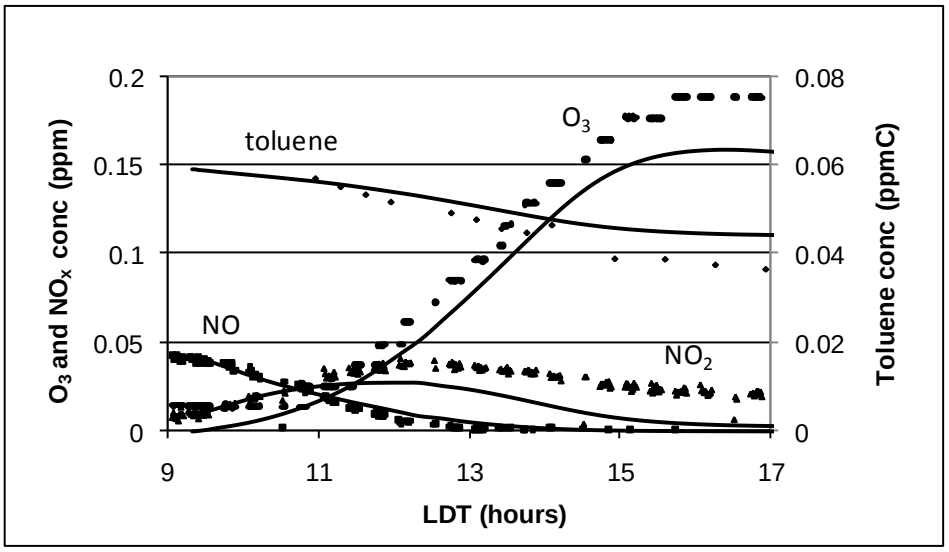

Figure 13. Comparison of model simulated and measured concentrations of NO_x, O_3, and toluene for 021508N experiment. The solid lines (—) represent model simulations. The circles are measured O_3; triangles are measured NO_2; squares are measured NO; diamonds are measured toluene.

The injection of SO_2 in the model was simulated by rapidly introducing SO_2 at the desired rate and then terminating the injection. In one instance (020808), multiple injections of SO_2 were conducted and modeled. As shown in Figure 14, the overall the fit of SO_2 was good (+/- 10%). Since the O_3, NO, NO_2, SO_2, and toluene fits were reasonable overall (+/- 30%), and would thereby give reasonable estimates of the hydroxyl radical concentration, H_2SO_4 predictions were possible. In addition, measurements collected using the denuder-filter

sampling train with ion chromatography confirms that total sulfate was in the same order of magnitude of model-predicted H_2SO_4. See Appendix B for model predictions for all experiments.

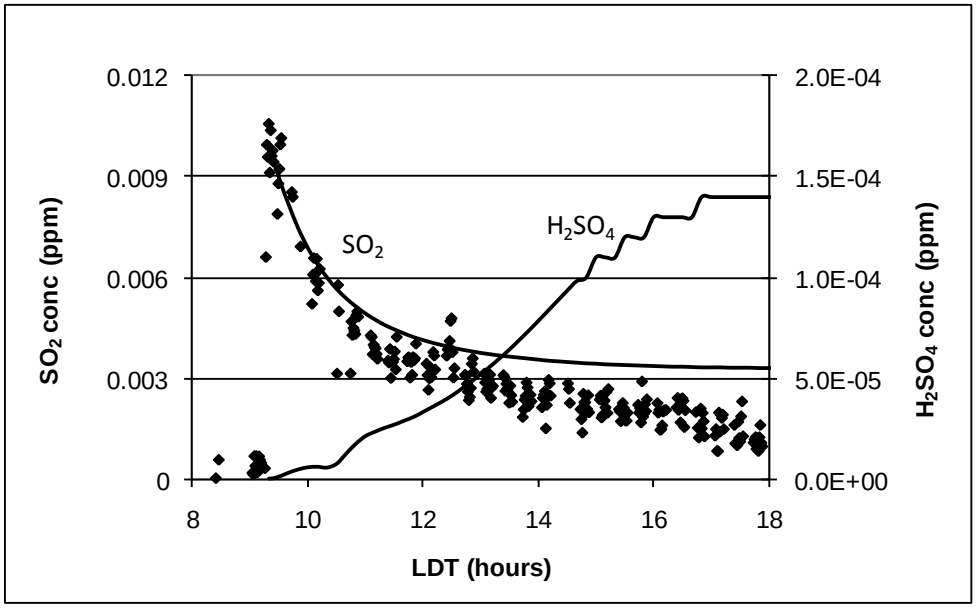

Figure 14. Comparison of model simulated and measured concentrations of SO_2 and H_2SO_4 for 021508N experiment. The solid lines (—) represent model simulations. The diamonds are measured SO_2.

Number of Stable Nuclei

Review of H_2SO_4 nucleation suggests the rate at which observable atmospheric stable nuclei are generated may be approximated by a direct function of $[H_2SO_4]_{gas}$ to some power between one and two. A pre-exponential factor on the $[H_2SO_4]$ term is used to describe the additional impact of organics (McMurry, 2006), as given in equation 1:

$$\#\text{ stable nuclei} = A\,[H_2SO_4]^x \qquad \text{where } 1 < x < 2 \qquad (eq.\ 1)$$

Recent analysis of field measurements of nucleation suggests that organic vapors could in fact contribute to particle nucleation (Kulmala *et al*., 2004, Kanakidou 2005). And many studies conclude that organics can directly and indirectly affect the growth of freshly nucleated particles (Zhang and Wexler, 2002; Anttila and Kerminen, 2003; Kulmala *et al*., 2004b, Kanakidou *et al*., 2005). To investigate the contribution of organic vapors to the initial nucleation of particles in the chamber-simulated urban environment, the fit of the number of stable nuclei was expanded include the contribution of organic vapors. And since the extent of partitioning for any organic compound between the gas and particulate phases depends not only on the on the amounts and properties of the compound, but is also a function of the amount of water in the atmosphere (Kanakidou *et al*., 2005), the inclusion of a water coefficient was also included in the analysis.

A reasonable hypothesis given the above is as follows:

$$\#\ \text{stable nuclei} = A\,[\Delta\text{tol}]^x[H_2SO_4]^y[H_2O]^z \qquad (\textit{eq. 2})$$

$$\text{Where } \Delta\text{tol} = [\text{toluene}]_i - [\text{toluene}]_f$$

To examine the number of stable nuclei generated in each system, experimental data were analyzed only during the time when the particle concentration increased, *i.e*., during the growth phase. Particle growth during the coagulation phase was not considered for this analysis. For each experiment, log-log multiple regressions were performed for the number of particles measured versus $[H_2SO_4]_{predicted}$, $[\Delta\text{tol}]_{predicted}$, and $[H_2O]_{measured}$ using a simple statistics package. The experiment conducted on 020808 was excluded from this analysis because the experimental methodology differed from the others. As shown in Appendix B, SO_2 was injected twice on 020808N. Although the experimental data for the five

experiments could be statistically fit to equation (2), the sulfuric acid term could explain 73-90% of the variability in the data, as shown in Table 6.

Table 6. Fits of # stable nuclei = A $[H_2SO_{4\ gas}]$ for each experiment

Date	Fit (# stable nuclei =)	r^2 adj.	p
101307N	$(1.1 \times 10^{12} \pm 4.5 \times 10^{6}) [H_2SO_4]^{(1.9\pm1.6)}$	77.3%	<0.05
102107N	$(8.7 \times 10^{14} \pm 5.0 \times 10^{4}) [H_2SO_4]^{(2.6\pm1.1)}$	89.5%	<0.05
021508N	$(3.2 \times 10^{10} \pm 8.7 \times 10^{5}) [H_2SO_4]^{(1.2\pm1.1)}$	72.7%	<0.05
030608S	$(7.0 \times 10^{9} \pm 2.2 \times 10^{3}) [H_2SO_4]^{(1.2\pm0.7)}$	82.0%	<0.05
030608N	$(1.5 \times 10^{9} \pm 3.3 \times 10^{3})[H_2SO_4]^{(1.2\pm0.9)}$	73.4%	<0.05
031308S	$(1.0 \times 10^{24} \pm 2.4 \times 10^{10})[H_2SO_4]^{(3.6\pm1.9)}$	90.1%	<0.05

If the data from all of the experiments were included in a single general equation of fit in the form of equation (1), the resulting equation 3, has an adjusted r^2 value of 0.15 and $p<0.05$, indicating that the general form of equation 1 does not sufficiently capture the variability in the five experiments.

$$\text{\# stable nuclei} = (5.1 \times 10^{5} \pm 2.2 \times 10^{1})[H_2SO_4]^{(0.4\pm0.3)} \qquad (\textit{eq. 3})$$

A better fit could be determined by using a linear form instead of an exponential. The linear best fit is given in equation 4; adjusted $r^2 = 0.50$ and $p < 0.05$. Figure 15 provides all of the data for the individual experiments and the predicted number of stable nuclei given by equations 3 and 4.

$$\#\text{ stable nuclei} = (2.1 \times 10^8 \pm 7.5 \times 10^7)[H_2SO_4] + (1.0 \times 10^4 \pm 5.9 \times 10^3) \qquad (eq.4)$$

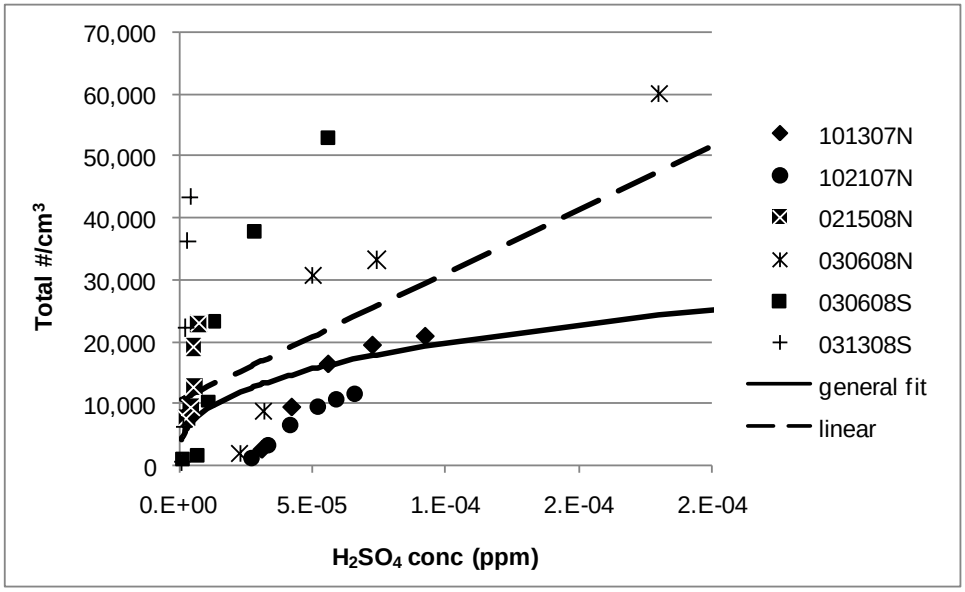

Figure 15. Measured number of stable nuclei for individual experiments. The "general fit" line is equation 3; "linear" dashed line is equation 4.

In a binary H_2SO_4 - water system, the nucleation rate has been shown to depend heavily on temperature relative humidity, and H_2SO_4 (Seinfeld & Pandis, 1998; Kulmala & Laaksonen, 1990; Jaecker-Voirol & Mirabel, 1989; Wexler *et al*.., 1994). An additional approach was used to see if a generalized model for the number of stable nuclei could be developed as a function of [Δtol], [H_2SO_4], [H_2O], temperature, and relative humidity. For each experiment, multiple step-wise linear and log-log regressions were performed on the data in order to determine the best fit (highest r^2) with a significance level of $p<0.05$ for all terms. For all of the experiments, no significant fit could be determined to be a function of water, temperature,

or relative humidity – leaving only [Δtol] and [H_2SO_4]. In many cases, the inclusion of water and temperature often led to a higher r^2 value for the equation of fit; however, the additional terms did not meet statistical significance requirements. Table 7 provides the individual equations of best fit for each experiment. Figure 15 illustrates an example of the general equation of fit (equation 3), the experiment-specific best fit in the form of equation 1, and the best possible equation of fit (in Table 7) for a single experiment.

Table 7. Best fits of # stable nuclei for all experiments. P(overall and each term)<0.05

Date	Fit (# stable nuclei =)	R^2 adj.
101307N	$(1.1 \times 10^{12} \pm 4.5 \times 10^{6})\ [H_2SO_4]^{(1.9\pm1.6)}$	77.3%
102107N	$(8.7 \times 10^{14} \pm 5.0 \times 10^{4})\ [H_2SO_4]^{(2.6\pm1.1)}$	89.5%
021508N	$(2.0 \times 10^{6} \pm 4.8)\ [\Delta tol]^{(0.7\pm0.2)}$	96.2%
030608S	$(7.0 \times 10^{9} \pm 2.2 \times 10^{3})\ [H_2SO_4]^{(1.2\pm0.7)}$	82.0%
030608N	$(8.0 \times 10^{8} \pm 6.1 \times 10^{1})\ [H_2SO_4]^{(4.6\pm2.6)}[\Delta tol]^{(-4.8\pm3.6)}$	94.9%
031308S	$(1.6 \times 10^{10} \pm 4.2 \times 10^{9})[H_2SO_4] - (1.9 \times 10^{4} \pm 1.2 \times 10^{4})$	97.1%

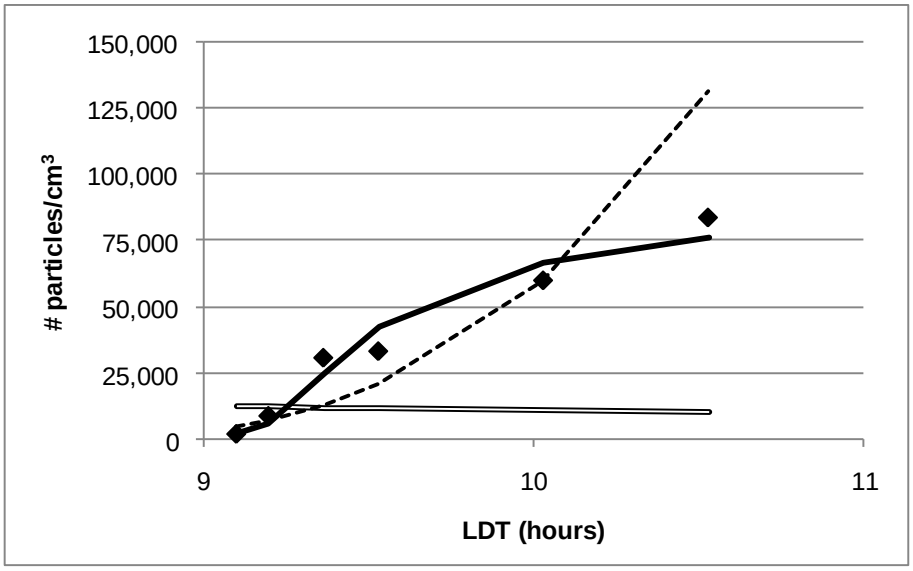

Figure 16. Equations of fit for # stable nuclei for 030608N. Diamonds represent SMPS measurements of total number of particles/cm^3. Double-dashed line (==) is the general equation of fit: # stable nuclei = 6.2 x 10^3 $[H_2SO_4]^{-0.07}$; single dashed line (- -) is: # of stable nuclei = 11.5 x 10^9 $[H_2SO_4]^{1.2}$; the solid line is the equation of best fit, # stable nuclei = 8.0 x 10^8 $[H_2SO_4]^{4.6}[\Delta tol]^{-4.8}$.

The results from the five experiments conducted indicate that a single equation of fit of general form of equation 1 cannot significantly represent the formation of stable nuclei in a complex urban atmosphere. However, for each individual experiment a unique equation of fit given by equation 1 could significantly capture 73-90% of the variability in the number of nuclei data. Since there is unknown uncertainty in the model-predicted concentrations of sulfuric acid (sulfuric acid is difficult to measure in the smog chamber), additional development of the model and field measurements are recommended. Based on statistical analysis of experimental and modeling data, no significant relationship could be found between the number of stable nuclei and water, temperature, or relative humidity. Although the inclusion of water and temperature in the equations of fit did not meet the significance level criteria, additional experimentation and a more robust data set with more frequent

temperature and water measurements may provide additional insight into the role of water and temperature in particle formation in an urban setting.

In most instances, a burst of particles was observed by SMPS within an hour of SO_2 injection in which 1,000 to 10,000 additional particles cm^{-3} appeared within minutes. For experiments in which it was possible to observe the initial burst in particles along with model predictions of H_2SO_4, the amount of gas-phase sulfuric acid predicted at the instant of the particle burst ranged from a concentration of 0.002 – 0.03 ppb (4.6×10^7 to 7.9×10^8 molecules cm^{-3}) with an average of 0.02 ± 0.01 ppb. Recent ground-based and aircraft measurements of nucleation events noted that nucleation events occurred under a variety of atmospheric conditions in which the concentration of H_2SO_4 ranged from approximately 1×10^6 to 6×10^7 molecules cm^{-3} (Lovejoy *et al.*, 2004). These field measurements further indicate that our model predictions of sulfuric acid are reasonable.

Particle Mass

To provide a rapid indicator of particle mass in almost real time, particle distribution measurements taken by SMPS were converted to particle mass by multiplying particle size by a density of 1.4 g cm^{-3} (Hu *et al.*, 2007; Bahreini *et al.*, 2005). National field studies have found that sulfate can often comprise up to 25% of fine particle mass, but the studies do not often provide real-time fine particle composition and growth information (Blanchard *et al.*, 2007). For the six chamber experiments, predicted $[H_2SO_4]_{gas}$ was compared to the time evolution of observed particle mass. In most instances, the predicted generation of $[H_2SO_4]$ occurs at the same time at which particle growth is observed; however, the $[H_2SO_4]$ does not account for all of the observed mass. Figure 17 illustrates the contribution of sulfuric acid to

the early growth of fine particle mass (6 nm < particles < 220 nm) during the 031308N experiment. Here, 5-20% of the fine particle mass during the initial burst of particles was composed of sulfuric acid, supporting the theory that SO_2 is important for initial particle formation and growth. If all of the model generated H_2SO_4 appears in the particle phase, then sulfate would contribute 5 to 25% of the initial burst of the particle phase, depending on the concentrations of the reaction species and the actual reaction time.

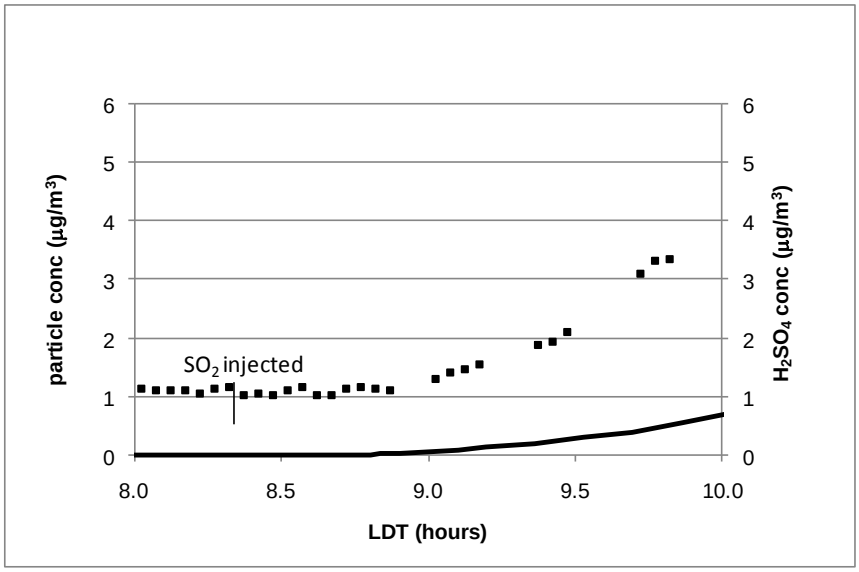

Figure 17. Comparison of model simulated H_2SO_4 and measured particle mass (6 nm < particles < 200 nm) for 030608N experiment. The solid line (—) represents model simulation. The squares are measured particle mass.

The fraction of water and the composition of the SOA species in the SMPS mass are unknown. Particle-phase components of the photooxidation of toluene in the absence of SO_2 have been theorized to include glyoxal oligomers, ketene oligomers from the photolysis of the toluene OH reaction product 2-methyl-2,4-hexadienedial, organic nitrates, methyl nitro-phenol analogues, C7 organic peroxides, acylperoxy nitrates, and unsaturated hydroxy nitro acids (Hu *et al*., 2007). Since the initial burst of particles appears in conjunction with rise in

the predicted H_2SO_4, we believe that inorganic acids catalyze the growth. As observed in the experiments that do not contain sulfuric acid, particle growth is observed throughout the day due to the condensation of organic vapors and potentially water. Additional work is needed to discern the contribution of gas-phase sulfuric acid, water, and SOA formation and growth in the urban atmosphere. Recent laboratory experiments conducted with aromatics and inorganic acid seed aerosols in the absence of NO_x suggest that particle acidity increases SOA yields (Cao & Jang, 2007). Further experimentation by Kleindienst *et al*. suggests that SO_2 may play a role in increasing the yield of secondary organic carbon from the photooxidation products of α-pinene and isoprene (Kleindienst *et al*., 2006). The results from the six realistic urban atmosphere experiments conducted at the UNC Aerosol Smog Chamber support that the SOA growth in this system can be enhanced by the addition of sulfur dioxide.

Suggested future work includes investigating the composition of the recently nucleated particles by advanced particle-phase mass spectrometry and conducting focused relative humidity smog chamber experiments. Sulfur dioxide-propylene-NOx experiments should be conducted so that DMA volumes and associated masses can be composed to model-predicted H2SO4. These experiments would eliminate confounded SOA, because propylene-NOx systems do not generate SOA. A DMA technique that employs sampling through a heated manifold (Kalberev *et al.*, 2004) could be used to determine the mass contribution of water by vaporizing the water (only) off of the particles. Finally, the relationship of particle acidity and growth by organics could be explored by the development of a kinetic SOA model that incorporates both particle formation by aromatic ozonolysis and by acid-catalyzed nucleation.

Conclusions

Experiments and photochemical modeling of a realistic urban atmosphere containing atmospherically relevant concentrations of ozone, oxides of nitrogen, urban hydrocarbons, sulfur dioxide, and existing particles support the theory that stable nucleation and growth in the daytime urban atmosphere is related to gas-phase sulfuric acid. Particle mass collected in the study indicates that both sulfuric acid and aromatic compounds can contribute to SOA mass; however, the interactive relationship of the two should be further explored. For individual experiments, the number of stable nuclei generated in the chamber experiments may be approximated by an exponential fit of sulfuric acid and in some cases, toluene. And preliminary analysis suggests that nucleation rates may be approximated by a linear equation involving gas phase sulfur dioxide. Overall, if all of the model generated H_2SO_4 appears in the particle phase, then sulfate would contribute 5 to 25% of the initial burst of the particle phase, depending on the concentrations of the reaction species and the actual reaction time.

APPENDIX A

PHOTOCHEMICAL MECHANISM

```
Title=Carbon Bond 4.2 + UNCCHAM.RXN;
!*********************************************************************
UNITS:
 Afactor=ppm_min;
IgnoreSpecies:
 CO2 ;
! I == INORGANIC CHEMISTRY
  { a) NO2 photolysis }
TABLE= HVNO2;
REACTIONS=
 Ia1]    NO2   = NO   + O                      # HVNO2   ,
 Ia2]    O  {+ O2   + M   } = O3  {+ M   }      # 83830 @ 1175. ,
Ia3]     O3   + NO  = NO2 {+ O2  }              # 2.643E+03 @-1370. ,
Ia4]     O   + NO2 = NO  {+ O2  }               # 1.375E+04 ,
Ia5]     O   + NO2 {+ M   } = NO3 {+ M   }      # 230.284 @ 687. ,
Ia6]     O   + NO  {+ M   } = NO2 {+ M   }      # 323.31  @ 602. ;
          { b) NO3 CHEMISTRY }
TABLES= HVNO3NO, HVNO3NO2;
REACTION=
Ib1]     O3   + NO2  = NO3  + O2                # 176.00 @-2450. ,
```

Ib2a] NO3 {hv} = NO + O2 # HVNO3NO ,

Ib2b] NO3 {hv} = NO2 + O # HVNO3NO2 ,

Ib3] NO3 + NO = 2.0*NO2 # 19086 @ 250 ,

Ib4] NO3 + NO2 = NO + NO2 # 36.6 @-1230 ,

Ib5] NO3 + NO2 {+ M } = N2O5 {+ M } # 784.88 @ 256 ,

Ib6] N2O5 {+ M } = NO3 + NO2 {+M } # 2.11E+16 @-10897,

Ib7] N2O5 + H2O = 2.0*HNO3 # 2.96E-6; {homogeneous rate only}

{ c) OZONE photolysis }

TABLES= HVO3O3P, HVO3O1D;

COEFF= fIc34=1E-5; {used to lower stiffness for O1D}

REACTIONS=

Ic1] O3{hv} = O + O2 # HVO3O3P ,

Ic2] O3{hv} = O1D + O2 # HVO3O1D ,

Ic3] O1D {+ M } = O + O2 # 1.147E10 @ 390 * fIc34 ,

Ic4] O1D + H2O = 2.0*OH # 3.26E5 * fIc34 ,

{above rates were multiplied by 1E-5 to lower stiffness}

Ic5] O3 + OH = HO2 + O2 # 2343.8 @-940 ,

Ic6] O3 + HO2 = OH + 2*O2 # 21.0 @-580 ;

{SO2 CHEMISTRY from Stockwell 1991 chemistry; walls are from rk}

TABLES=walladj;

REACTIONS=

ISX1] SO2 + WALLSO2sites = SO2walls # 1E-2*{walladj},

ISX2] WALLSO2sites = # 1E-2{1.5E-2},

ISX3] SO2 + OH = SO3 + HO2 # 1370,

ISX3b] HO2 + SO2 = OH + SO3 #1.3, {Mallard et al 1993}

ISX4] SO3 + H2O +H2O = H2SO4 # 1E-8,

ISX6A] SO3 = WALLSO2sites # 4e-3,

ISX6] H2SO4 + WALLSO2sites = # 4E-2;

{ d) HONO CHEMISTRY }

COEFF= HONO_NO2R=0.171; {from ratio of rates on July 13, 1986 UNC Site}

REACTIONS=

Id1] NO + NO {+ O2} = 2.0*NO2 # 2.60E-5 @ 530 ,

Id2] NO + NO2 + H2O = 2.0*HONO # 1.6E-11 ,

Id3] HONO + HONO = NO + NO2 +H2O # 1.5E-5 ,

Id4] OH + NO {+ M } = HONO {+ M} # 655.44 @ 806 ,

Id5] HONO = OH + NO # HVNO2 * HONO_NO2R ,

Id6] OH + HONO = NO2 + H2O # 9770

{ e) NO/NO2 with RO2}

REACTIONS=

Ie1] HO2 + NO = OH + NO2 # 5482.1 @ 242 ,

```
Ie2]    HO2  + NO2 {+ M } = PNA {+ M }      # 164.0 @ 749 ,
Ie3]    PNA  {+ M } = HO2 + NO2 {+M}       # 2.876E+15 @-10121 ,
Ie4]    OH   + PNA = NO2 {+H2O  + O2}       # 1909 @ 380 ,
Ie5]    OH   + NO2 {+ M} = HNO3             # 1536.78 @ 713 ,
Ie6]    OH   + HNO3  = NO3                  # 7.6 @ 1000 ;
        ! f) HO2 TERMINATION REACTIONS
TABLE=HVH2O2;
REACTIONS=
If1]    HO2  + HO2 = H2O2 + O2                      # 87.39 @ 1150 ,
If2]    HO2  + HO2 + H2O  = H2O2 + O2 + H2O         # 7.69E-10 @ 5800 ,
If3]    H2O2 = 2*OH                                 # HVH2O2
If4]    OH + H2O2   = HO2 + H2O                     # 4719.8 @-187 ,
If5]    OH + CO {+ M} = HO2  + CO2                  # 322.0 ,
If6]    OH + CH4  = XO2 + HCHO + HO2                # 3.55E+3 @-1710;
! ***** C1 == FORMALDHYDE CHEMISTRY****
TABLE= HVHCHOR, HVHCHOS ;
REACTIONS=
C1_1]  HCHO {hv}= 2*HO2 + CO                # HVHCHOR ,
C1_2]  HCHO   {hv}= CO  + H2                # HVHCHOS ,
C1_3]  HCHO + OH   = HO2   + CO             # 15000 ,
```

C1_4] HCHO + O = OH + HO2 + CO # 43019.2 @-1550 ,

C1_5] HCHO + NO3 = HNO3 + HO2 + CO # 0.93 ;

{ C2 == HIGHER ALDEHYDE CHEMISTRY }

TABLE= HVCCHOr;

REACTIONS=

C2_1] CCHO = XO2 + 2*HO2 + CO + HCHO # HVCCHOr ,

C2_2] CCHO + O = C2O3 + OH # 17394.7 @-986 ,

C2_3] CCHO + OH = C2O3 # 10372.2 @ 250,

C2_4] CCHO + NO3 = C2O3 + HNO3 # 3.7 ;

!

! In rxns below assume that RCHO species is same as CCHO

SpeciesAlias:RCHO=CCHO;

{ MG == DICARBONYL CHEMISTRY }

TABLE= HVMetGly,HVGLYH2,HVGLYHO2;

REACTIONS=

MG_1] MGLY = 0.9*C2O3 + 0.9*HO2 + 0.9*CO + 0.1*CCHO + 0.1*CO # HVMetGly, {CB4 2002}

MG_1] GLY = 0.4*HO2+ 0.4*CO + 0.80*HCHO + 0.8*CO # HVGLYHO2, {CB4 2002}

MG_2] OH + MGLY = C2O3 + CO + HO2 # 1359@828 , {CB4 2002}

MG_2] OH + GLY = 0.2 * C2O3 + 1.6*CO + 0.8*HO2 # 16839; {'H-CO-CO-OO.' is lumped into C2O3 in CB42002 mech at 298 K }

{ PAN CHEMISTRY }

REACTIONS=

PAN_1] C2O3 + NO = NO2 + XO2 + HCHO + HO2 # 7915.0 @ 250 ,

PAN_2] C2O3 + NO2 = PAN # 1.18e-4 @ 5500 ,{CB4 2002}

PAN_3] PAN = C2O3 + NO2 # 5.62e18 @-14000, {CB4 2002}

PAN_4] C2O3+ C2O3 = 2*XO2 + 2*HCHO + 2*HO2 # 3700 ,

PAN_5] C2O3+ HO2 = 0.79*HCHO + 0.79*XO2 + 0.79*HO2 + 0.79*OH # 9600 ;

IgnoreSpecies:

KETENE, NTR, XO2N;

{ PARAFFIN CHEMISTRY }

REACTIONS=

PAR_1] OH + PAR = 0.87*XO2 + 0.13*XO2N + 0.11*HO2 + 0.11*RCHO+ 0.76*ROR + -0.11*PAR # 1203.0 ,

PAR_2] ROR = 1.1*RCHO + 0.96*XO2 + 0.94*HO2 + -2.1*PAR + 0.04*XO2N + 0.02*ROR # 6.2495E+16 @-8000 ,

PAR_3] ROR = HO2 + KETENE # 95455 ,

PAR_4] ROR + NO2 = NTR # 22000 ,

PAR_5] OH + MEOH = HCHO + HO2 # 1.98E+04@-805 ;

{ ETHENE CHEMISTRY }

REACTIONS=

ETH_1] O + C:C = HCHO + 0.70*XO2 + CO + 1.70*HO2+ 0.30*OH # 15400 @-792 ,

ETH_2] OH + C:C = XO2 + 1.56*HCHO + HO2 + 0.22*RCHO # 3000 @ 411 ,

ETH_3] O3 + C:C = HCHO + 0.42*CO + 0.12*HO2 # 18.56 @-2633 ;

{ OLEFIN CHEMISTRY }

REACTIONS=

OLE_1] O + OLE = 0.63*RCHO + 0.38*HO2 + 0.28*XO2 + 0.30*CO+ 0.20*HCHO + 0.02*XO2N + 0.22*PAR + 0.20*OH # 17560.0 @-324 ,

OLE_2] OH + OLE = HCHO + RCHO + XO2 + HO2 + -1*PAR # 7740.0 @ 504 ,

OLE_3] O3 + OLE = 0.5*RCHO + 0.74*HCHO + 0.33*CO + 0.44*HO2+ 0.22*XO2 + 0.10*OH + -1.0*PAR # 21.04 @-2105 ,

OLE_4] NO3 + OLE = 0.91*XO2 + 0.09*XO2N + HCHO + RCHO + -1*PAR+ NO2 # 11.35 ;

{#if ISOP

{ ISOPRENE CHEMISTRY--CONDENSED }

ISO_1] O + ISOP = 0.6*HO2 + 0.80*RCHO + 0.55*OLE + 0.50*XO2 + 0.50*CO + 0.45*C:C + 0.9*PAR # 27000 ,

ISO_2] OH + ISOP = XO2 + HCHO{+ 0.05*PAR} + 0.67*HO2 + 0.13*XO2N + 1.0*C:C + 0.4*MGLY + 0.2*C2O3 + 0.2*RCHO # 142000 ,

ISO_3] O3 + ISOP = HCHO + 0.4*RCHO + 0.55*C:C + 0.2*MGLY+ 0.10*PAR + 0.06*CO + 0.44*HO2 +0.1*OH # 0.018 ,

ISO_4] NO3 + ISOP = XO2N # 470 ;}

#end

{ TOLUENE CHEMISTRY – EXPLORATORY KAMENS MODEL, 2008 }

{COEFF OPEN_NO2R=0.021;}

REACTIONS=

TOL_1] OH + TOL = 0.64*TO2 + 0.1*benzald + 0.28*XO2 + 0.36*HO2 + 0.18*CRES +0.072*OH + 0.08*MeHexdial # 2740 @338, {Calvert,p 47}

TOL_2] acyl-ene + TOL = HO2 + CCHO {+ tol-epox} #100,

{as per Di, 2007 peroxyacyl attack on toluene}

TOL_3] TO2 + NO = {0.14*NO2-Aro} 0.86*TOLO # 12000 ,

TOL_4] NO3 + TOL = 0.65*TO2 + 0.1*benzald + 0.28*XO2 +0.72*HNO3 + 0.36*HO2 {+ 0.28*NO2-Aro} +0.08*OH + 0.07*MeHexdial # 0.103, {Calvert p, 139}

TOL_5] benzald + OH = 0.95*BZO-oo + 0.05*TO2 # 1.91E4, {Calvert,p 71}

TOL_6] BZO-oo + NO2 = BZPAN #1.2E-4@5500,

TOL_7] BZPAN = NO2 + BZO-oo #1.27e18@-13600, {Calvert,p 108}

TOL_8] TOLO = 0.64*c4dial + 0.36*c5dial+0.45*MGLY+ 0.55*GLY +HO2 # 1e6, {to be consistent with Di bt not representing MBUT}

TOL_9] OH + CRES = {0.4*CRO +} 0.6*NO2MePhenol +0.60*XO2 + 0.60*HO2 + 0.30*TOLO +-0.6*NO2 # 61000 ,

TOL_10] NO3 + CRES = 0.6*XO2 +0.6*NO2MePhenol + 0.6*TOLO # 32500 ,

TOL_10a] OH + MeHexdial = 0.6*MGLY + 0.6*c4dial+0.4*GLY +0.4*c5dial + XO2 + HO2 # 8.38E4, {calvert 225}

TOL_11] c4dial +O3 = 0.5*GLY +HO2 + 0.1*OH + 0.5*polycarb {+0.2*C2O3} # 0.015, {Calvert, 210}

TOL_12] c5dial +O3 = 0.25*GLY +0.25*MGLY +HO2 + 0.1*OH + 0.5*polycarb {+0.2*C2O3} # 0.015, {Calvert, 210}

TOL_13] c4dial + OH = 0.3*GLY + 0.5*HO2 + 0.6*XO2 + 0.2*OHcarbNO3 +-0.2*NO+ 0.5*Maleic +0.15*polycarb + 0.1*acyl-ene # 8.38E4,{Calvert206}

TOL_14] c5dial + OH = 0.2*pent-oo +0.5*pent-rad +0.1*acyl-ene + 0.2*OHcarbNO3 +-0.2*NO # 8.38E4,{Calver 206}

TOL_15] c4dial = 0.5*HCHO {+0.5*XO2} +0.5*HO2 {+0.6*Acr}+ 0.2*acyl-ene # HVMETGLY,

TOL_16] c5dial = 0.5*HCHO {+0.5*XO2} + 0.5*HO2 { 0.7*Acr} +0.2*acyl-ene # HVCCHOr{HVMETGLY} ,

TOL_17a] acyl-ene +NO2 = C4enePAN # 1.18e-4 @ 5500 ,{CB4 PAN 2002}

TOL_18b] C4enePAN = acyl-ene +NO2 # 5.62e18 @-14000, {CB4 PAN}

TOL_17] pent-oo= XO2 + 0.5*GLY+ 0.5*MGLY + 0.5*CO+ 0.5*HO2 {+0.25*OHoxybutal} +0.5*polycarb {+0.25*but-tricarb} # 1E6,

{TOL_18] OHoxybutal + OH = HCHO + polycarb +XO2 # 1000,

TOL_19] but-tricarb + OH = HCHO + polycarb +XO2 # 1000,}

TOL_20] pent-rad = Maleic + 1.5*XO2 + HO2 + HCHO # 1E6,

Tol_21] Maleic +OH = 0.8*Malo-oo {0.2*CO2} # 2.07E3,

Tol_22] Malo-oo +NO = 0.2*OHcarbNO3 + 0.8*polycarb+0.8*XO2 +0.8*HO2 #12000,

TOL_23] Malo-oo + HO2= carb-acid # 635,

TOL_24] pent-oo + pent-oo = polycarb + 0.6*carb-acid+1.4*XO2 + 1.4*HO2{+1.4CO2} # 25111 @416,

TOL_25] pent-oo +HO2 = carb-acid + O3 # 635,

TOL_26] pent-oo + XO2 = 1.6*MGLY +XO2 +HO2 {+CO2} # 7522 @272,

TOL_27] TO2 + pent-oo = 1.4*carb-acid {+2CO2} # 7522 @272,

TOL_28] TO2 + HO2 = aro-acid # 310 @1320,

TOL_30] TO2 + XO2 = aro-acid # 7522 @272,

TOL_31] TO2 + TO2 = aro-acid #7522 @272;

{ XYLENE CHEMISTRY }

REACTIONS=

{XYL_1] OH + XYL = 0.70*HO2 + 0.50*XO2 + 0.20*CRES + 0.80*MGLY+ 1.10*PAR + 0.30*TO2 # 24527.56 @ 116;} {CB4}

XYL_2] OH + oXYL = 0.5*TO2 + 0.4*MGLY+ PAR +0.05*benzald + 0.28*XO2+ 0.36*HO2 + 0.10*CRES +0.072*OH + 0.15*MeHexdial

19900,{Calvert,p 51}

XYL_3] acyl-ene + oXYL = HO2 + CCHO {+ xol-epox} #80; {as per Di, 2007 peroxyacyl attack on toluene}

{operator Chemistry}

REACTIONS=

XO_1] XO2 + NO = NO2 # 4431@280,

{XO_2] XO2N + NO = {NTR} # 1000.0 ,}

XO_3] XO2 + XO2 = # 369@190,

XO_4] XO2 + HO2 = # 561@800;

Wloss4] seed {walls} = # 0.0006,

Wloss5] GLYpoly {walls} = # 0.0006,

Wloss5] O3 {walls} = # 0.0001,

! Include the Mechanism Independent Chamber Wall reactions

#def CB4

@%MECH%unccham.rxn

EndMechanism

APPENDIX B

MODEL RESULTS

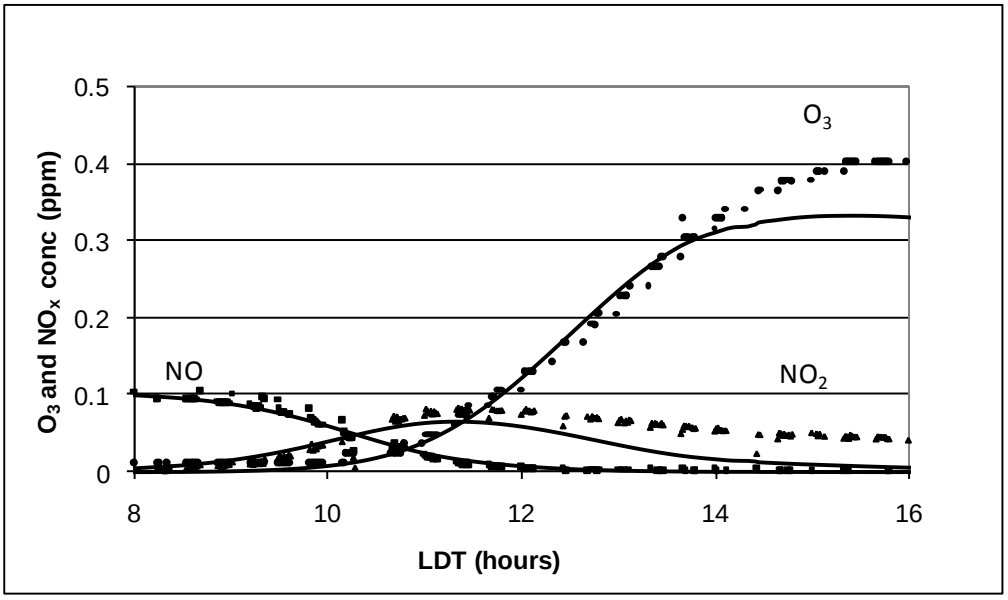

Figure A-1. Comparison of model simulated and measured concentrations of NO_x and O_3 for 101307N experiment. The solid lines (—) represent model simulations. The circles are measured O_3; triangles are measured NO_2; squares are measured NO.

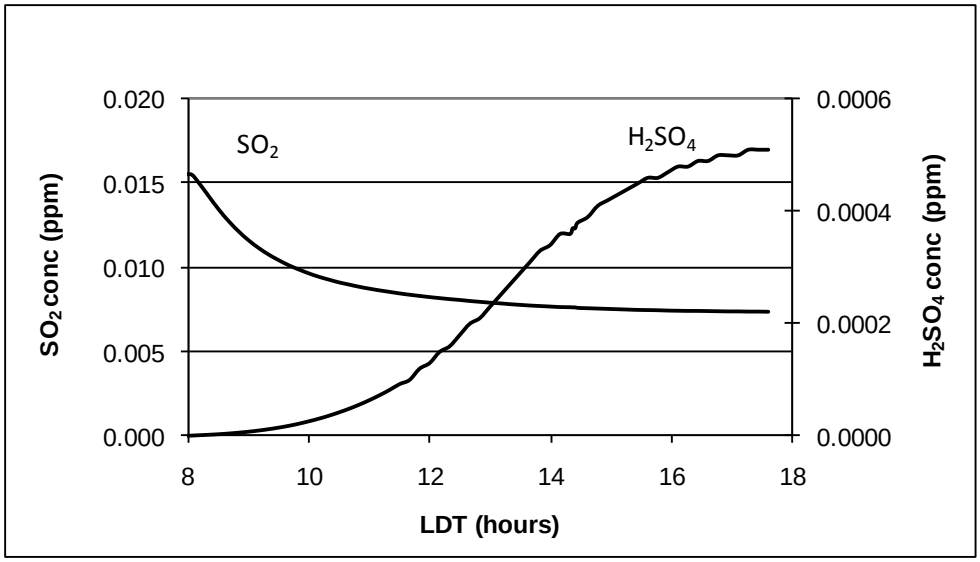

Figure A-2. Model simulated concentrations of SO_2 and H_2SO_4 for 101307N experiment. SO_2 measurements were not available for this experiment.

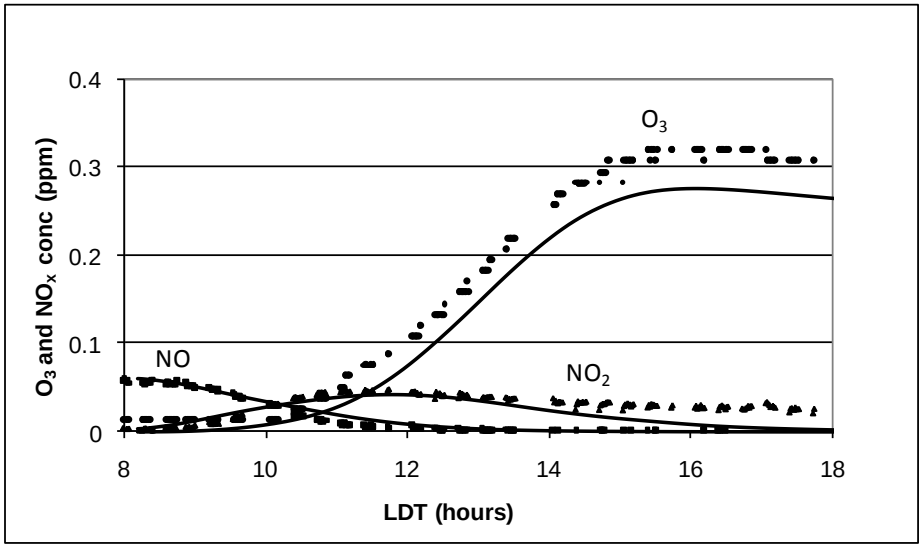

Figure A-3. Comparison of model simulated and measured concentrations of NO_x and O_3 for 102107N experiment. The solid lines (—) represent model simulations. The circles are measured O_3; triangles are measured NO_2; squares are measured NO.

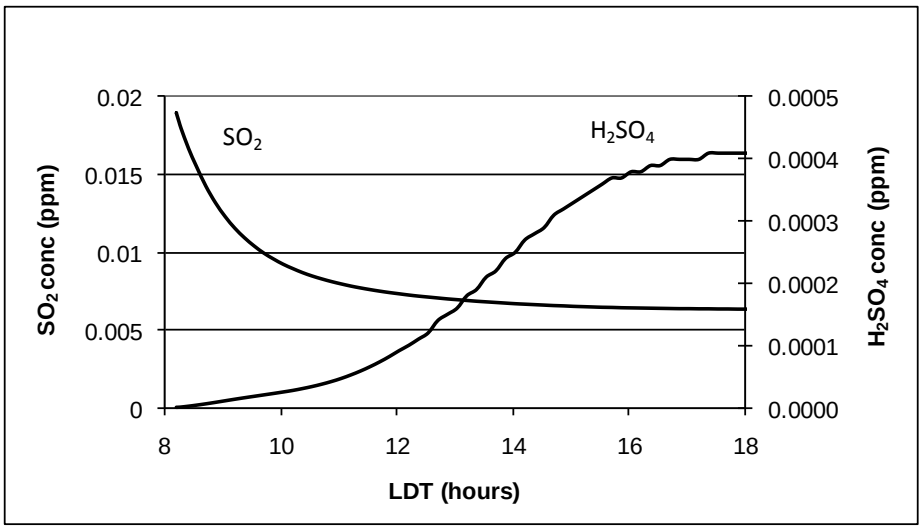

Figure A-4. Model simulated concentrations of SO_2 and H_2SO_4 for 101307N experiment. SO_2 measurements were not available for this experiment.

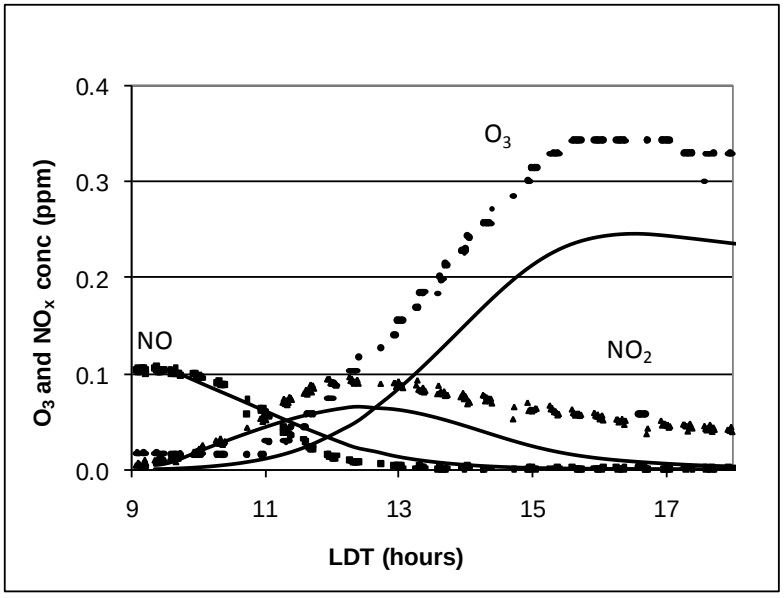

Figure A-5. Comparison of model simulated and measured concentrations of NO_x and O_3 for 020808N experiment. The solid lines (—) represent model simulations. The circles are measured O_3; triangles are measured NO_2; squares are measured NO.

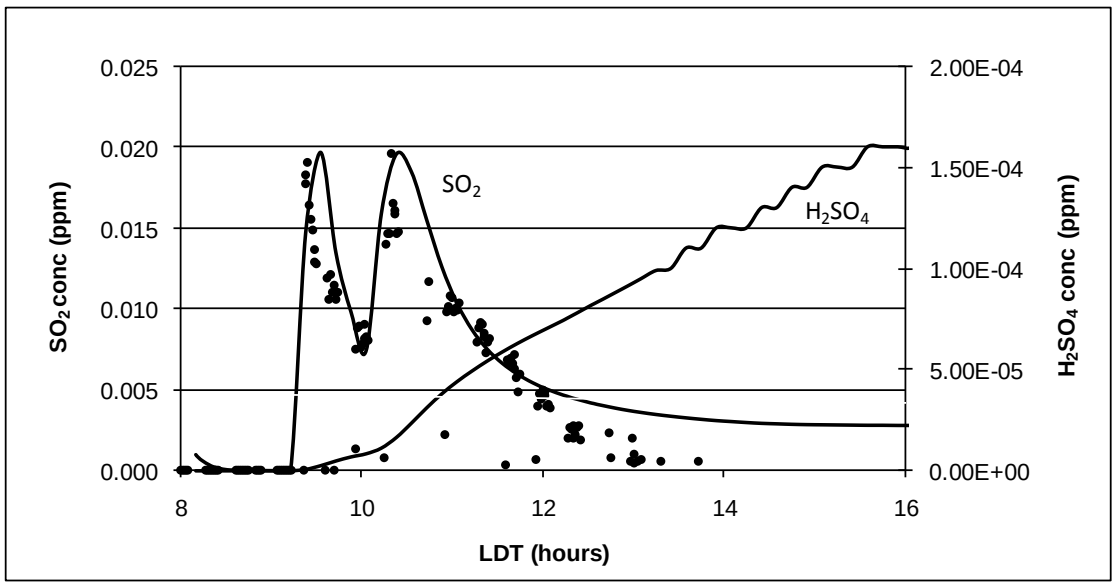

Figure A-6. Comparison of model simulated and measured concentrations of SO_2 and H_2SO_4 for 02808N experiment. The solid lines (—) represent model simulations. The circles are measured SO_2. Initial injection of 0.02 ppm SO_2 at 9:20, second injection of 0.01 ppm SO_2 at 10:15. SO_2 wall loss ~ 0.1 $ppm^{-1}min^{-1}$.

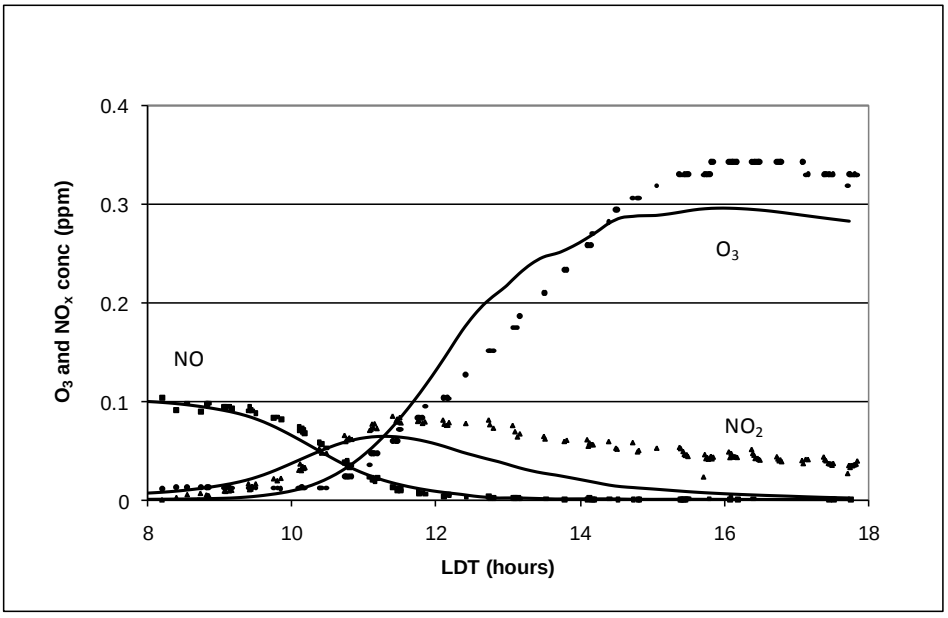

Figure A-7. Comparison of model simulated and measured concentrations of NO_x and O_3 for 030608N experiment. The solid lines (—) represent model simulations. The circles are measured O_3; triangles are measured NO_2; squares are measured NO.

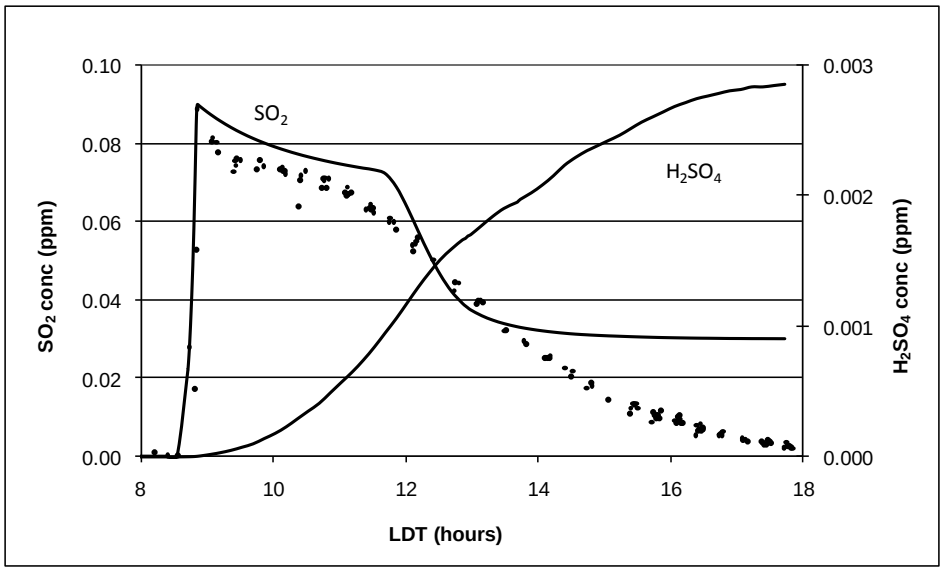

Figure A-8. Comparison of model simulated and measured concentrations of SO_2 and H_2SO_4 for 030608N experiment. The solid lines (—) represent model simulations. The circles are measured SO_2

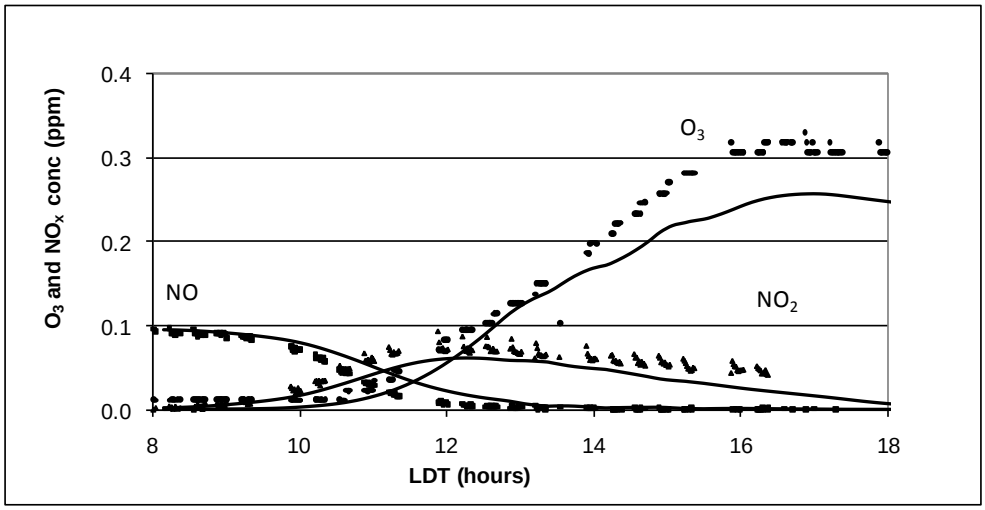

Figure A-9. Comparison of model simulated and measured concentrations of NO_x and O_3 for 030608S experiment. The solid lines (—) represent model simulations. The circles are measured O_3; triangles are measured NO_2; squares are measured NO.

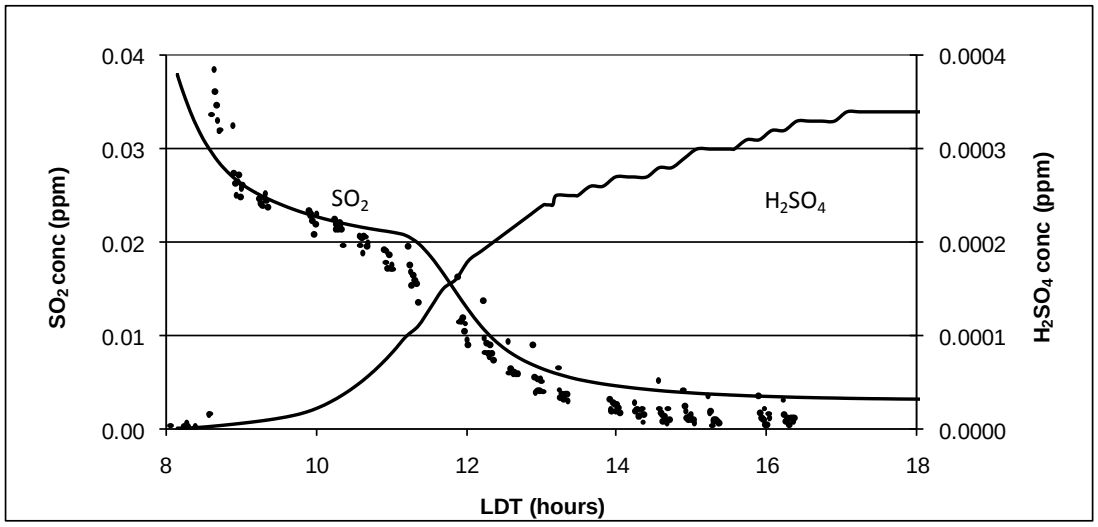

Figure A-10. Comparison of model simulated and measured concentrations of SO_2 and H_2SO_4 for 030608S experiment. The solid lines (—) represent model simulations. The circles are measured SO_2

APPENDIX C

CPC CALIBRATION

The two condensation particle counters are routinely calibrated for sizing ability by measuring the diameter of polystyrene latex spheres (PSLs) of a known diameter. The following chart illustrates the calibration of the primary CPC.

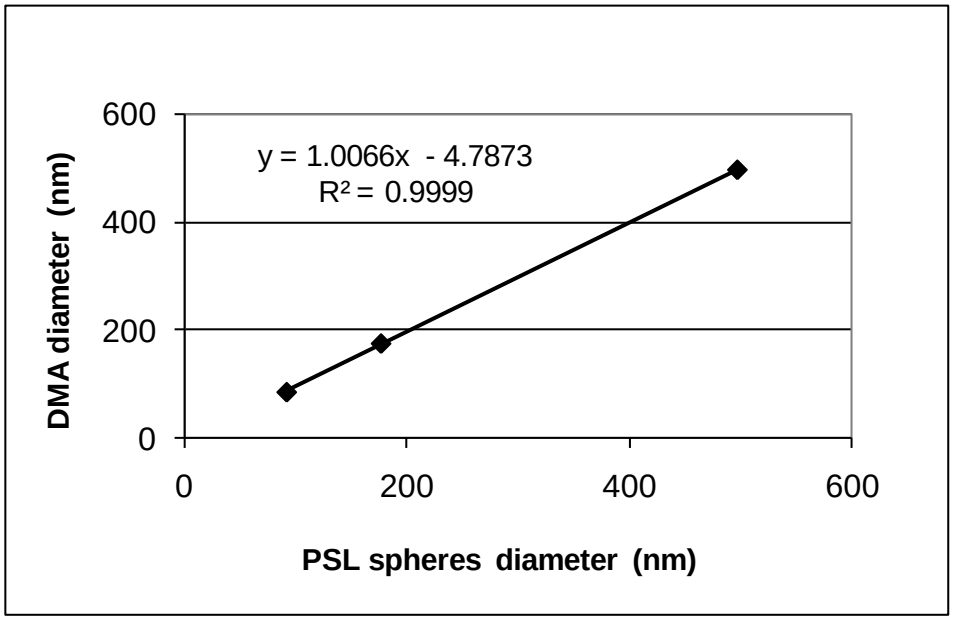

Figure C-1. Diameter of measured PSL spheres vs. known PSL diameter. Diamonds represent measurements; solid line is a linear regression.

APPENDIX D

IC SULFATE ANALYSIS

During three experiments (020808, 021508, and 030608), samples were also taken for gravimetric mass and inorganic ions. For the determination of the gravimetric mass, particle sulfate samples were collected simultaneously by a denuder-filter sampling train that consists of two annual denuders in series coated with a solution of 1% Na_2CO_2, 1% glycerin in a 50:50 mixture of H_2O:methanol in the first and 1% citric acid, 1% glycerin in methanol in the second, followed by particle collection on a 47 mm Teflon filter. This system removed gas-phase sulfate from the air stream and facilitated analysis of particle-phase (only) sulfate via ion chromatography (Possanzini *et al.*, 1983; EPA, 1988). Following the mass measurements, the Teflon filters were extracted in 3 mL of deionized water and analyzed for their ionic contents with an ion chromatograph (model 4500-i, Dionex Corp, Sunnyvale, CA) with electrical conductivity detection and anion suppression. Anions were separated with an IonPac AS41-SC column and an isocratic 1.7 mM sodium bicarbonate /1.8 mM sodium carbonate eluent as specified in EPA Method 9056A, Determination of Inorganic Anions by Ion Chromatography.

Results for the 020808 and 021508 experiments were inconclusive due to an insufficient amount of particle mass collected on the filters. Figure B-1 presents ion chromatography data for 030608N/S experiments.

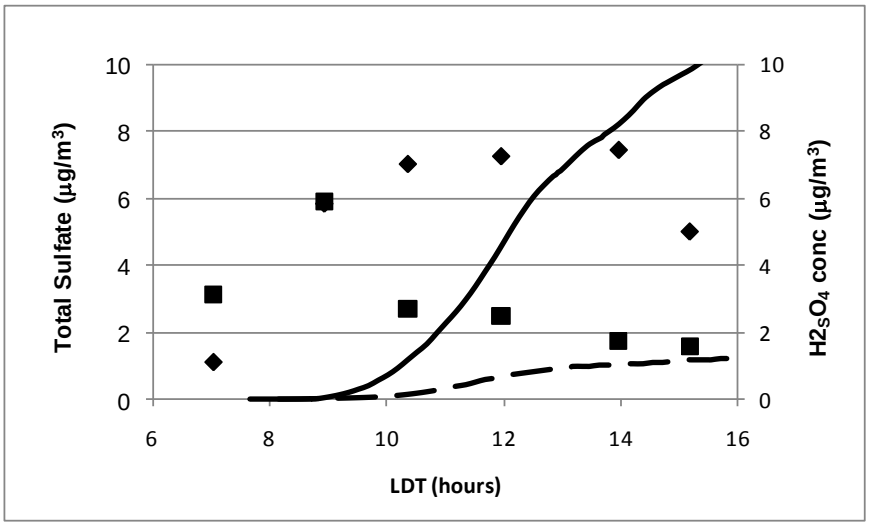

Figure B-1. Total sulfate measured by ion chromatography and predicted concentration of sulfuric acid for 030608N/S. Squares represent ion chromatography measurements for the North; diamonds for the South. Solid line represents predicted [H_2SO_4] for North; dashed line for the South.

WORKS CITED

Agarwal, J.K. and G.J. Sem. "Generating Submicron Monodisperse Aerosols for Instrument Calibration." *TSI Quarterly*, Vol. 4, No. 2 – May-June, pp 3-8.

Altieri, K.E., Carlton, A.G., Lim, H., Turpin, B.J., Seitzinger, S.P. Evidence for Oligomer Formation in Clouds: Reactions of Isoprene Oxidation Products. *Environmental Science and Technology*, 40, 4956-4960, 2006.

Anttila, T. and Kerminen, V. M.: Condensational growth of atmospheric nuclei by organic vapours, *J. Aerosol Sci*., 34, 41–61,2003.

Appel BR, Tanner RL, Adams DF, et al. Semi-continuous determination of atmospheric particulate sulfur, sulfuric acid, and ammonium sulfates (Method 713). Lodge JP, ed. Methods of air sampling analysis. 3rd ed. Chelsea, MI: Lewis Publishers, Inc. 529-532, 1987.

ATSDR Toxicological Profile for Sulfur Trioxide and Sulfuric Acid. US Department of Health and Human Services, Public Health Service, Agency for Toxic Substances and Disease Registry, 1998.

Bahreini, R., Keywood, M.D., Ng, N.L., Varutbangkul, V., Gas, S., Flagan, R.C., Seinfeld, J.H., Worsnop, D.R., Jimenez,J.L. Measurements of secondary organic aerosol from oxidation of cycloalkenes, terpenes, and m-xylene using an aerodyne aerosol mass spectrometer. *Environmental Science and Technology* 39 (15), 5674–5688, 2005.

Blanchard, C.L.; Tanenbaum, S.; Hidy, G.M. Effects of Sulfur Dioxide and Oxides of Nitrogen Emission Reductions on Fine Particulate Matter Mass Concentrations: Regional Comparisons. *J. Air & Waste Manage. Assoc*., 57:1337-1350, 2007.

Bonn, B. and Moortgat, G. K.: New particle formation during alpha- and beta-pinene oxidation by O3, OH and NO3, and the influence of water vapour: particle size distribution studies, *Atmos. Chem. Phys*., 2, 183–196, 2002.

Broyles, D.A., Carpenter, B.K. Experimental detection of one case of benzene epoxidation by a peroxy radical and computational prediction of another. Journal of Organic Chemistry 70 (21), 8642–8644, 2005.

Calvert, Jack G., Atkinson, Roger et al., 2002: The mechanisms of atmospheric oxidation of aromatic hydrocarbons.

Carter, W.P.L., Atkinson, R., Winer, A.M., Pitts, J.N.J. Evidence for chamber-dependent radical sources: impact on kinetic computer models for air pollution. International Journal of Chemical Kinetics 13 (8), 735–740, 1981.

Gang Cao and Myoseon Jang. Effects of particle acidity and UV light on secondary organic aerosol formation from oxidation of aromatics in the absence of NOx . *Atmospheric Environment*, (41), 7603-7613, 2007.

Clarke, A.D., Davis D., Kapustin V.N., Eisele F., Chen G., Paluch I., Lenschow D., Bandy A.R., Thornton D., Moore K., Mauldin L., Tanner D., Litchy M., Carroll M.A., Collins J., and Albercook, G., Particle nucleation in the tropical boundary layer and its coupling to marine sulfur sources. *Science*, 282 89-92, 1998.

Doyle, G.J. Self-nucleation in the sulfuric acid-water system. *J. Chem. Phys.*, 35, 795-799, 1961.

Edney, E.O., Driscoll, D.J., Weathers, W.S., Kleindienst, T.E., Conver, T.S., McIver, C.D., Li, W. Formation of polyketones in irradiated toluene/propylene/NOx/air mixtures. *Aerosol Science and Technology* 35 (6), 998–1008, 2001.

Eisele, F.L. McMurry, P.H., Recent progress in understanding particle nucleation and growth." Phil. Trans. R. Soc. Lond. B, 1997. 352, 191-201, 1997.

Environmental Protection Agency (EPA): The Science of Annular Denuders (a Tutorial), 1988.

Gery, M. W., Whitten, G. Z., Killus, J. P., and Dodge, M. C.: A photochemical kinetics mechanism for urban and regional scaled computer modeling, J. *Geophys. Res.*, 94, 12 925–12 956, 1989.

Gao, S., Hegg, D. A., Frick, G., Caffrey, P. F., Pasternack, L., Cantrell, C., Sullivan, W., Ambrusko, J., Albrechcinski, T., and Kirchstetter, T. W. Experimental and modelling studies of secondary organic aerosol formation and some applications to the marine boundary layer, *J. Geophys. Res.*, 106, 27 619–27 634, 2001.

Gaydos, T., Stanier, C. O., and Pandis, S. N. Modelling new particle formation events during the Pittsburgh Air Quality Study, *J. Geophys. Res.*, in press, 2004.

Hinds, William C., Aerosol Technology, 2nd Ed., Wiley, New York, 1999.

Hu, Di; Tolocka, M.; Li, Q; Kamens, R. A kinetic mechanism for predicting secondary aerosol formation from toluene oxidation in the presence of NOx and natural sunlight. *Atmospheric Environment.* 41:6478-6496, 2007.

Intergovernmental Panel on Climate Change (IPCC): Climate Change: The Scientific Basis, Cambridge University Press, UK, 2001.

A. Jaecker-Voirol, P. Mirabel, and H. Reiss, *J. Chem. Phys.* 87, 4849,1987.

Jeffries, H., Fox, D., and Kamens, R. Outdoor Smog Chamber Studies: Effects of

Hydrocarbon Reduction on Nitrogen Dioxide. US EPA – 650/3-75-011, 1975.

Jeffries, H. E. PC-Photochemical Kinetics Simulation System (PC-PKSS), Software Version 3.0; Department of Environmental Sciences and Engineering, School of Public Health: University of North Carolina, Chapel Hill, NC 27599, 1991.

Jeffries, H., Sexton, K., Adelman, Z. Auxiliary mechanisms (wall models) for UNC outdoor chamber. EPA/600/R-00/076, 1999.

Jeffries, H.E., Kessler, M., Gery, M., 2003. Mcomp/meval: the morphecule photochemical reaction mechanism. 2003

Janson, R., Rosman, K., Karlsson, A., and Hansson, H. C.: Biogenic emissions and gaseous precursors to forest aerosols, Tellus B, 53, 423–440, 2001.

Kamens, R. M., Jang, M., Chien, C. J., and Leach, K.: Aerosol formation from the reaction of alpha-pinene and ozone using a gas phase kinetics-aerosol partitioning model, *Environ. Sci. Technol*., 33, 1430–1438, 1999.

Kamens, R. M. and Jaoui, M.: Modelling aerosol formation from a-pinene + NOx in the presence of natural sunlight using gasphase kinetics and gas-particle partitioning theory, *Environ. Sci. Technol*., 35, 1394–1405, 2001.

Kanakidou, M.; Seinfeld, J. H.; Pandis, S. N.; Barnes, I.; Dentener, F. J.; Facchini, M. C.; van Dingenen, R.; Ervens, B.; Nenes, A.; Nielsen, C. J.; Swietlicki, E.; Putaud, J. P.; Balkanski, Y.; Fuzzi, S.; Horth, J.; Moortgat, G. K.; Winterhalter, R.; Myhre, C. E. L.; Tsigaridis, K.; Vignati, E.; Stephanou, E. G.; Wilson, J. Organic aerosol and global climate modelling: a review. *Atmos. Chem. Phys. Discuss*. 2004, 4 5855-6024, 2005.

Katz, J.L. Condensation of a supersaturated vapor. I. The homogeneous nucleation of the n-alkanes, *J. Chem. Phys*., 52, 4733-4748, 1994.

Killus, J.P., Whitten, G.Z. Background reactivity in smog chambers. International *Journal of Chemical Kinetics* 22 (6), 547–575, 1990.

Kleindienst, T.E., Conver, T.S., McIver, C.D., Edney, E.O. Determination of secondary organic aerosol products from the photooxidation of toluene and their implications in ambient PM2.5. *Journal of Atmospheric Chemistry* 47 (1), 79–100, 2004.

Kleindienst, T.E.; Edney, E.O.; Lewandowski, M; Offenberg, J.H., and Jaoui, M. Secondary Organic Carbon and Aerosol Yields from the Irradiations of Isoprene and alpha-Pinene in the Presence of NO*x* and SO2, *Environ. Sci. Technol*., 40, 3807–3812, 2006.

Kulmala, Markku. How Particles Nucleate and Grow, *Science*, 302 1000-1001, 2003.

Kulmala, M., and Laaksonen, A. Binary nucleation of water-sulfuric acid system comparison of classical theories with different H2SO4 saturation vapor pressures, *J. Chem. Phys*, 93, 696-701, 1990.

Kulmala, M., Hameri, K., Aalto, P. P., Makela J. M., Pirjola, L., Nilsson, E. D., Buzorius, G., Rannik, U., Dal Maso, M., Seidl, W., Hoffman, T., Janson, R., Hansson, H. C., Viisanen, Y., Laaksonen, A., and O'Dowd, C. D.: Overview of the international project on biogenic aerosol formation in the boreal forest (BIOFOR), Tellus B, 53, 324–343, 2001.

Kulmala, M.; Vehkama¨ki, H.; Peta¨ja¨, T.; Dal Maso, M.; Lauri, A.; Kerminen, V.-M.; Birmili, W.; McMurry, P. H. *J. Aerosol. Sci.* **2004**, *35*,143.

Lee, S., Jang, M., Kamens, R.M. SOA formation from the photooxidataion of a-pinene in the presence of freshly emitted diesel soot exhaust. *Atmospheric Environment* 38, 2597–2605, 2004.

Leungsakul, S., Jeffries, H.E., Kamens, R.M. A kinetic mechanism for predicting secondary aerosol formation from the reactions of D-limonene in the presence of oxides of nitrogen and natural sunlight. *Atmospheric Environment* 39 (37), 7063–7082, 2005a.

Leungsakul, S., Jaoui, M., Kamens, R.M. Kinetic mechanism for predicting secondary organic aerosol formation from the reaction of D-limonene with ozone. *Environmental Science and Technology* 39 (24), 9583–9594, 2005b.

Lim, H., Carlton, A.G., Turpin, B.J. Isoprene from Secondary Organic Aerosol through Cloud Processing: Model Simulations. *Environmental Science and Technology,* 39, 4441-4446, 2005.

Lioy PJ, Waldman JM. Acidic sulfate aerosols: Characterization and exposure. *Environ Health Perspect* 79: 15-34, 1989.

Lovejoy, E.R.; Curtius, J.; Froyd, K.D. Atmospheric ion-induced nucleation of sulfuric acid and water. *Journal of Geophysical Research*, 109: D08204 , 2004.

Mallard, W. G., Westley, F., Herron, J. T., Hampson, R. F., and Frizzell, D. H. NIST Chemical Kinetics Database-Ver 5.0, *NIST Standard Reference Data*, Gaithersburg, MD, 1993.

McMurry, P.H., Report from "New Particle Formation" Breakout Session, NARSTO Workshop on PM Simulation and Process Evaluation, quoting Carslaw and coworkers, and Kulmala and coworkers Boulder, June, 2006.

Mihalopoulos, N.; Kerminen, V.M.; Kanakidou, M.; Berresheim, H.; Sciare, J. Formation of particulate sulfate species (sulfate and methanesulfonate) during summer over the

Eastern Mediterranean: A modelling approach, *Atmospheric Environment* (41), 6860-6871, 2007.

T. Novokov and J.E.Penner. Large contribution of organic aerosols to cloud-condensation nuclei concentrations, Letters to *Nature*, 365, 823-826.

Odum, J.R.; Hoffmann, T.; Bowman, F.; Collins, D.; Seinfeld, J.H. Gas/Particle Partitioning And Secondary Organic Aerosol Yields, *Environmental Science and Technology,* 3, 2580-2585, 1996.

Pankow, J.F. An absorption model of gas/particle partitioning of organic compounds in the atmosphere. *Atmospheric Environment* 28, 185–188, 1994.

Pitts, B.J and Pitts, J.N. Chemistry of the Upper and Lower Atmosphere: Theory, Experiments, and Applications. Academic Press, San Diego, 2000.

Possanzini, M.; Febo, A.; Liberti, A. New Design of a High-Performance Denuder for the Sampling of Atmospheric Pollutants. *Atmospheric Environment* (17:12), 2605-2610, 1983.

Seinfeld, John H. Atmospheric Chemistry and Physics of Air Pollution. John Wiley & Sons, Inc. NY, 1986.

Seinfeld, J.H., Pandis, S.N. Atmospheric Chemistry and Physics from Air Pollution to Climate Change. John Wiley & Sons, Inc., NY, 1998.

Stockwell et al., "The Second-Generation Regional Acid Deposition Model Chemical Mechanism for Regional Air Quality Modeling, *J. Geophys. Res*., 95D, 16, 343-16, 367, 1990.

Voicu, I. A Revised Carbon Bond Mechanism. The University of North Carolina at Chapel Hill, Department of Environmental Sciences and Engineering, 2003

M. Volmer and A. Weber, Zh. Fiz. Khim. 119, 277, 1926.

Weber, R.J.; McMurray; P.H.; Eisele, F.L.; Tanner, D.J. Measurement of Expected Nucleation Precursors and 3-500 nm Diameter Particles at Mauna Loa Observatory, Hawaii. *Journal of Atmospheric Sciences*. 52:12, 2242-2257, 1995.

Went, F. W.: Blue hazes in the atmosphere, *Nature*, 187, 641–643,1960.

Wexler, A. S., Lurmann, F.W., and Seinfeld, J. H.: Modelling urban and regional aerosols-I. Model development, *Atmos. Environ*., 28, 3, 531–546, 1994.

Zhang, K. M. and Wexler, A. S.: A hypothesis for growth of fresh nuclei, *J. Geophys. Res*., 107, 4577, 2002.